Earth **Surface**
Dynamics

EGU

# [10]Be systematics in the Tsangpo-Brahmaputra catchment: the cosmogenic nuclide legacy of the eastern Himalayan syntaxis

**Maarten Lupker[1,6], Jérôme Lavé[2], Christian France-Lanord[2], Marcus Christl[3], Didier Bourlès[4], Julien Carcaillet[5], Colin Maden[6], Rainer Wieler[6], Mustafizur Rahman[7], Devojit Bezbaruah[8], and Liu Xiaohan[9]**

[1]Geological Institute, D-ERDW, ETH Zürich, Zürich, 8092, Switzerland
[2]CRPG, UMR 7358 CNRS–Univ. de Lorraine, Vandoeuvre les Nancy, 54500, France
[3]Institute of Particle Physics, D-PHYS, ETH Zürich, Zürich, 8093, Switzerland
[4]CEREGE, UMR 34 UAM-CNRS-IRD, Aix-en-Provence, 13545, France
[5]ISTerre, Univ. Grenoble Alpes–CNRS, Grenoble, 38000, France
[6]Institute of Geochemistry and Petrology, D-ERDW, ETH Zürich, Zürich, 8092, Switzerland
[7]Department of Soil, Water and Environment, Dhaka University, Dhaka, 1000, Bangladesh
[8]Department of Applied Geology, Dibrugarh University, Dibrugarh, 786004, India
[9]Institute of Tibetan Plateau Research, Chinese Academy of Sciences, Beijing, China

*Correspondence to:* Maarten Lupker (maarten.lupker@erdw.ethz.ch)

**Abstract.** The Tsangpo-Brahmaputra River drains the eastern part of the Himalayan range and flows from the Tibetan Plateau through the eastern Himalayan syntaxis downstream to the Indo-Gangetic floodplain and the Bay of Bengal. As such, it is a unique natural laboratory to study how denudation and sediment production processes are transferred to river detrital signals. In this study, we present a new [10]Be data set to constrain denudation rates across the catchment and to quantify the impact of rapid erosion within the syntaxis region on cosmogenic nuclide budgets and signals. The measured [10]Be denudation rates span around 2 orders of magnitude across individual catchments (ranging from 0.03 to $> 4\,mm\,yr^{-1}$) and sharply increase as the Tsangpo-Brahmaputra flows across the eastern Himalaya. The increase in denudation rates, however, occurs $\sim 150\,km$ downstream of the Namche Barwa–Gyala Peri massif (NBGPm), an area which has been previously characterized by extremely high erosion and exhumation rates. We suggest that this downstream lag is mainly due to the physical abrasion of coarse-grained, low [10]Be concentration, landslide material produced within the syntaxis that dilutes the upstream high-concentration [10]Be flux from the Tibetan Plateau only after abrasion has transferred sediment to the studied sand fraction. A simple abrasion model produces typical lag distances of 50 to 150 km compatible with our observations. Abrasion effects reduce the spatial resolution over which denudation can be constrained in the eastern Himalayan syntaxis. In addition, we also highlight that denudation rate estimates are dependent on the sediment connectivity, storage, and quartz content of the upstream Tibetan Plateau part of the catchment, which tends to lead to an overestimation of downstream denudation rates. While no direct [10]Be denudation measurements were made in the syntaxis, the dilution of the upstream [10]Be signal, measured in Tsangpo-Brahmaputra sediments, provides constraints on the denudation rates in that region. These denudation estimates range from ca. 2 to $5\,mm\,yr^{-1}$ for the entire syntaxis and ca. 4 to $28\,mm\,yr^{-1}$ for the NBGPm, which is significantly higher than other large catchments. Overall, [10]Be concentrations measured at the outlet of the Tsangpo-Brahmaputra in Bangladesh suggest a sediment flux between 780 and $1430\,Mt\,yr^{-1}$ equivalent to a denudation rate between 0.7 and $1.2\,mm\,yr^{-1}$ for the entire catchment.

## 1 Introduction

The large-scale and intense interaction between tectonics and climate make the Himalayan range the largest sediment source to the ocean. The Tsangpo-Brahmaputra is a major catchment draining the Himalayan range and the Tibetan Plateau. It is an exceptional natural laboratory to better understand how denudation processes are reflected in sedimentary load because of the large geomorphological diversity of its catchment. A remarkable feature of the Tsangpo-Brahmaputra catchment is the eastern Himalayan syntaxis. Interactions between tectonic and surface processes are most likely observed in tectonic syntaxes (Koons et al., 2013). The eastern Himalayan syntaxis has been proposed as a typical example of how active tectonic deformation, thermal weakening of the crust, and steep topography could be self-sustained by intense erosion and rapid exhumation of crustal material within the framework of the tectonic aneurysm model (Zeitler et al., 2001). Although the extent and nature of this coupling has recently been challenged (Bendick and Ehlers, 2014; Wang et al., 2014; King et al., 2016), there is ample evidence for superimposed rapid exhumation (Burg et al., 1998; Seward and Burg, 2008; Zeitler et al., 2014; Bracciali et al., 2016) and active erosion (Finlayson et al., 2002; Finnegan et al., 2008; Stewart et al., 2008; Enkelmann et al., 2011; Larsen and Montgomery, 2012; Lang et al., 2013) in a focused area around the Namche Barwa–Gyala Peri massif (NBGPm), where the course of the Tsangpo-Brahmaputra is marked by a sharp bend to the south-west (Fig. 1). Difficult access to the NBGPm means that contemporary denudation rates are poorly constrained, but estimates range from ca. 5 to 17 mm yr$^{-1}$ (Stewart et al., 2008; Enkelmann et al., 2011; Larsen and Montgomery, 2012). The NBGPm is thought to be responsible for up to 40 to 70 % of the sediment discharge of the entire Brahmaputra (e.g., Singh and France-Lanord, 2002; Garzanti et al., 2004), illustrating the potential for a small area of the Tsangpo-Brahmaputra to act as a major source of sediments to the entire river network. Upstream of the NBGPm, the Tsangpo-Brahmaputra drains the relatively flat, slowly eroding, and arid southern edge of the Tibetan Plateau, while the downstream part of the catchments includes a range of large Himalayan tributaries draining the eastern half of the Himalayan range and the Indo-Gangetic floodplain. In this work, we present a terrestrial cosmogenic nuclide (TCN), $^{10}$Be, data set spanning the entire Tsangpo-Brahmaputra catchment, covering the Tibetan Plateau downstream to the outlet in Bangladesh. The wide range of surface processes and rates of landscape evolution across the catchment represent a unique opportunity to study how these denudation signals are transferred through the catchment and integrated into the sedimentary load. The use of TCN also represents an opportunity to provide new quantitative con-

straints on the denudation rates across the catchment in general and the NBGPm in particular.

Cosmogenic nuclides have been widely used to constrain catchment-wide denudation rates (CWDRs) over a range of scales and catchment sizes (e.g., Portenga et al., 2011). The concentration of a given cosmogenic nuclide in river sediments theoretically reflects the rate at which the upstream landscape is lowering through physical erosion and chemical weathering assuming steady-state denudation (Brown et al., 1995; Bierman and Steig, 1996; Granger et al., 1996). However, it is also increasingly recognized that CWDRs are affected by a number of site-specific biases and limitations that prevent us from simply reading denudation rates from a bag of sand. Amongst others, landsliding, a dominant erosion process in actively eroding landscapes, violates the steady-state denudation assumption and may thus lead to biases in the CWDR (Niemi et al., 2005; Yanites et al., 2009). The stochastic nature of sediment supply to the channels and hydrology within the river network may also perturb the TCN signal over a range of timescales and limits our ability to use a single sediment sample as a representative and accurate representative of upstream erosion products (Kober et al., 2012; Lupker et al., 2012; West et al., 2014; Foster and Anderson, 2016). Glacial erosion is not properly accounted for, as sediments eroded under a glacier are shielded from cosmic rays and, hence, supply sediment with very low TCN concentrations independent of glacial erosion rates (Godard et al., 2012; Delunel et al., 2014). Different erosion processes also affect the final grain size of fluvially exported sediment, which may in turn lead to a grain size dependence of TCN signals that needs to be taken into account in order to derive robust CWDRs (Clapp et al., 2002; Belmont et al., 2007; Aguilar et al., 2014; Puchol et al., 2014; Lukens et al., 2016). The assumption of quartz ubiquity or content within the eroded lithology of a studied catchment is also likely to be violated in a number of cases and is also a source of biases in CWDR (Carretier et al., 2015a). Finally, large catchments, and especially floodplains, represent temporary storage compartments, in which TCN may accumulate or decay depending on storage duration and depth, which may in turn affect the TCN concentration in river sediments (Wittmann and von Blanckenburg, 2016). These limitations need to be properly evaluated in order to quantitatively relate TCN signals to surface processes and denudation rates. Since most of these limitations also apply to the Tsangpo-Brahmaputra, this study further represents a unique opportunity to evaluate and quantify the potential biases associated with the use of TCNs in large, actively eroding, and contrasted catchments.
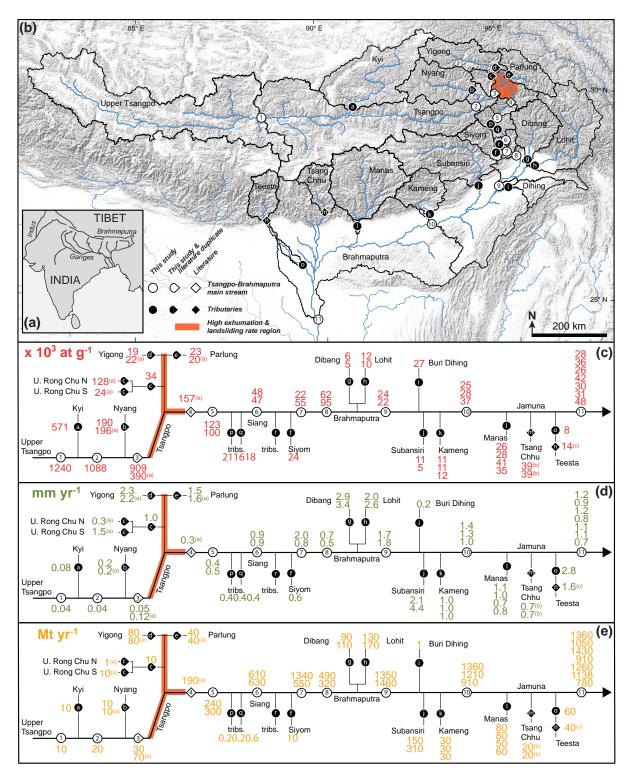
**Figure 1.** **(a)** Overview of the study area. **(b)** Shaded-relief map of the Tsangpo-Brahmaputra map with sampling locations of the trunk stream (open symbols) and main tributaries (filled symbols). The NBGPm area characterized by high erosion and fluvial incision rates ($> 3$ mm yr$^{-1}$) is highlighted in red (see text for references). $^{10}$Be concentrations **(c)**; $^{10}$Be-derived denudation rates **(d)**; $^{10}$Be-derived sediment fluxes **(e)** of Tsangpo-Brahmaputra main stream and tributaries. Downstream samples have been corrected for floodplain area by excluding areas below 300 m a.s.l. from the calculation. Literature data from Finnegan et al. (2008) **(a)**, Portenga et al. (2015) **(b)**, and Abrahami et al. (2016) **(c)** are also included.

## 2 Settings and methods

### 2.1 The Tsangpo-Brahmaputra catchment

The Yarlung–Tsangpo–Siang–Brahmaputra–Jamuna River system (as the trunk river is called from upstream to downstream, from now on referred to as the Tsangpo–Brahmaputra in this paper) is a large drainage basin of ca. 530 000 km$^2$, draining the eastern half of the Himalayan range. It originates close to Mount Kailash, in central Tibet, and flows eastward along the Indus-Tsangpo suture zone and the northern flank of the Himalayan range for about 1500 km. This part of the catchment is marked by a relatively flat topography and a high average elevation (> 4000 m a.s.l.). Being in the rain shadow of the Himalayan range, it receives little precipitation (< 500 mm yr$^{-1}$) and a significant part of the runoff is generated by snowmelt from the range to the north (Bookhagen and Burbank, 2010). The Tibetan part of the Tsangpo-Brahmaputra catchment is dominated by Paleozoic sedimentary sequences with the carbonate-rich Tethyan Sedimentary Series (TSS) and ultramafic to felsic rocks of the Trans-Himalayan batholiths and the Neotethys ophiolites (Liu and Einsele, 1994).

In the north-eastern part of the catchment, the Tsangpo-Brahmaputra River sharply bends to the south, leaves the Tibetan Plateau, and cuts through the Himalayan range through deep gorges and a prominent knickpoint, losing over 2000 m of elevation in less than 100 km of channel length. The NBGPm, and more generally the eastern Himalayan syntaxis, is marked by very steep topography and high relief resulting from the deflection of crustal material around the indenting Indian plate and the growth of a large antiformal metamorphic structure that is deeply dissected by active fluvial incision (Burg et al., 1997; Finnegan et al., 2008). This reach of the Tsangpo-Brahmaputra is underlain by gneiss, quartzites, marbles, and generally highly metamorphic rocks from the Higher Himalayan Crystallines (HHC) (Burg et al., 1997). Just south of the syntaxis, the river flows over the Abor volcanics as well as limestones and shales (Jain and Thakur, 1978; Acharyya, 2007). The large valley along the Tsangpo-Brahmaputra, south of the syntaxis, channels moisture and precipitation northwards, which translates into significant rainfall (> 2000 mm yr$^{-1}$) up to 100 km north of the Himalayan front in the syntax region (Anders et al., 2006; Bookhagen et al., 2006).

The Tsangpo-Brahmaputra exits the Himalayan range in Pasighat, Arunachal Pradesh, NE India, and finally discharges into the Bay of Bengal in Bangladesh after crossing the Assam and Indo-Gangetic alluvial floodplains for about 1000 km (Fig. 1). The main stream of the Tsangpo-Brahmaputra further receives input from the eastern Himalayan rivers Lohit and Dibang that drain the poorly documented Mishmi hill formations and from Himalayan rivers draining the southern flank of the eastern Himalayan range (Subansiri, Kameng, Manas, and Teesta rivers). The north-

ern tributaries of the Tsangpo-Brahmaputra drain the classical HHC and Lesser Himalayan units composed of a variety of crystalline and metasedimentary rocks, as well as the ca. mid-Miocene sub-Himalayan Siwalik molasses (Yin et al., 2006; Chirouze et al., 2012). Sediment input from the southern tributaries originating from the Shillong Plateau, as well as from the northern part of the Indo-Burman ranges, is thought to be small (Garzanti et al., 2004). The Indo-Gangetic floodplain and the southern flank tributaries to the Tsangpo-Brahmaputra receive intense precipitation (up to 4000 mm yr$^{-1}$), which mainly falls during the 4 months of the Indian summer monsoon (June to September) (Bookhagen and Burbank, 2010).

### 2.2 Sampling and analytical methods

River sediments were sampled from the Tibetan headwaters down to the Brahmaputra in Bangladesh, including the major tributaries. For sample locations upstream of the Himalayan front (Pasighat, pt. 8 in Fig. 1; all points hereafter can be referred to in Fig. 1 as well), sediments were taken from fresh sandbars. Downstream of the Himalayan front, river sediments were dredged in the center of the channel using local boats. A number of sampling points were revisited several years to assess the temporal variability in the [10]Be signal. After collection, samples were dried and sieved into several grain size fractions ranging from 63 to 1000 µm (Table S1 in the Supplement).

Grain size fractions were then separated with a Frantz magnetic separator and the nonmagnetic fraction was further treated with HCl (38 %) to remove carbonates. This fraction subsequently underwent four to five leachings (3 to 5 days each) in $H_2SiF_6$ (34 %) – HCl (38 %) (2/3–1/3 vol.) alternating agitation and heated ultrasonic bath treatments (70 °C). The purified quartz fractions were then further cleaned, to remove possible remaining meteoric [10]Be contributions, through three subsequent HF baths in stoichiometric amounts so as to dissolve 10 % of the total sample mass at each step. Chemical separation of the purified quartz was performed in the labs of ISTerre – Grenoble (TSA samples) and at the ETH Zürich (remaining samples). In both cases procedures were very similar. Purified quartz was dissolved in concentrated HF along with a small amount of [9]Be carrier solution (Table S1). Be was separated by ion-exchange chromatography, precipitated as $Be(OH)_2$, and dehydrated to BeO at 1000 °C (von Blanckenburg et al., 1996). Systematic procedural blanks were also separated using similar procedures.

[10]Be / [9]Be ratios were measured at different AMS (accelerator mass spectrometry) facilities: the 5 MeV ASTER AMS facility at CEREGE (Klein et al., 2008), the 6 MeV TANDEM AMS, and the 0.5 TANDY AMS of ETH Zürich (Christl et al., 2013). [10]Be / [9]Be ratios measured at the CEREGE were normalized to NIST 27900, with an assumed [10]Be / [9]Be ratio of $2.79 \times 10^{-11}$, while the [10]Be / [9]Be ra-

tios measured at ETH were normalized to the ETH standard S2007N, with an assumed ratio $2.81 \times 10^{-11}$ (Christl et al., 2013). Both normalization procedures are comparable and equivalent to the 07KNSTD standardization (Nishiizumi et al., 2007) with a $^{10}$Be half-life of 1.387 Ma (Chmeleff et al., 2010; Korschinek et al., 2010). Sample measurements were corrected for procedural blanks with $^{10}$Be / $^9$Be ratios ranging from 2.35 ($\pm 1.07$) $\times 10^{-15}$ to 7.99 ($\pm 2.17$) $\times 10^{-15}$ depending on measurement batch and date (Table S1).

Recent work from Portenga et al. (2015) suggests the possible occurrence of $^9$Be in the analyzed quartz aliquots despite careful cleaning and purification of the samples. About 3 g of purified quartz was dissolved in concentrated HF, dried down, and redissolved in a 2 % $HNO_3$ solution. The $^9$Be concentration of the solution was measured on a PerkinElmer SCIEX ELAN DRC-e quadrupole ICP-MS at ETH Zürich by standard-sample bracketing. This approach yielded consistent results compared to a subset of samples measured by standard addition, suggesting that ICP matrix effects are limited. The external reproducibility of the $^9$Be concentration measurements by standard-sample bracketing was ca. 10 % ($1\sigma$). For samples with enough material, replicate 3 g quartz splits were measured to assess the homogeneity of the $^9$Be concentration among different quartz aliquots.

In this study, we also included the $^{10}$Be data concentration data of large tributaries that were measured by Finnegan et al. (2008) on the upper part of the catchment as well as the Yigong and Parlung Zangbo rivers (pts. 3, 4, d and e), by Portenga et al. (2015) for samples of the Tsang Chhu (pt. m), and by Abrahami et al. (2016) for samples from the Teesta (pt. n). For consistency, the $^{10}$Be concentration data reported in these publications were re-processed using the same procedure as our data. Existing additional $^{10}$Be data within the Tsangpo-Brahmaputra catchment from Le-Roux-Mallouf et al. (2015) were not included in this study as they mainly focus on smaller, second-order catchments within the Bhutan Himalayas.

## 2.3 Catchment-wide denudation rate and sediment flux calculations

The procedure for the determination of basin-wide denudation rates using the TCN data is similar to that detailed in Lupker et al. (2012) and is summarized hereafter. All data are reported in Table S1. Basin average denudation rates, $\overline{\varepsilon}$ (cm yr$^{-1}$), were calculated from the measured $^{10}$Be concentration, $N$ (at g$^{-1}$), following Eq. (1) (Brown et al., 1995), thereby assuming efficient mixing of the sediments in the river system and steady-state denudation:

$$N = \frac{1}{\overline{\varepsilon}} \times \left( \frac{\overline{P_{n_i}}}{\mu_n} + \frac{\overline{P_{ms_i}}}{\mu_{ms}} + \frac{\overline{P_{mf_i}}}{\mu_{mf}} \right) = \frac{1}{\overline{\varepsilon}} \times \sum_i \frac{\overline{P_i}}{\mu_i}, \quad (1)$$

in which $\overline{P_{n_i}}$, $\overline{P_{ms_i}}$, and $\overline{P_{mf_i}}$ are the average basin-wide $^{10}$Be production rates (at g$^{-1}$ yr$^{-1}$) by neutrons, slow muons, and

fast muons, respectively. $\mu_i = \rho / \Lambda_i$ with $\rho$ is the average density of the eroded material (here 2.7 g cm$^{-3}$) and $\Lambda_i$ is the effective attenuation length of neutrons and slow and fast muons ($\Lambda_n \sim 160$, $\Lambda_{\mu s} \sim 1500$, and $\Lambda_{\mu f} \sim 4320$ g cm$^{-2}$; Braucher et al., 2011). Equation (1) implies that the radioactive decay of $^{10}$Be can be neglected compared to the denudation rate ($\overline{\varepsilon} \times \mu_i \gg \lambda$), which is the case for typical denudation rates in tectonically active areas.

The basin-wide $^{10}$Be production rate $\overline{P_i}$ was determined following Eq. (2):

$$\overline{P_i} = \frac{1}{S} \int \underset{x,y}{\int} P_i(x, y) \times F_{\text{topo}}(x, y)$$
$$\times F_{\text{glacier}}(x, y) \times \mathrm{d}x\mathrm{d}y, \quad (2)$$

in which $S$ is the basin area, $P_i(x, y)$ the local production rate at each point of the basin and $F_{\text{topo}}$ and $F_{\text{glacier}}$ are topographic and glacier correction factors integrated over the basin surface $S$. To calculate $P_i(x, y)$, the sea level high-latitude (SLHL) $^{10}$Be production rates by neutrons and slow and fast muons were scaled for latitude and local altitude according to Lal (1991) and Stone (2000) (St scaling scheme). For this work, we used the most recent nucleonic SLHL production rate of $4.01 \pm 0.10$ at g$^{-1}$ yr$^{-1}$ compiled by Phillips et al. (2016) and the slow and fast muonic contribution of Braucher et al. (2011). Given the high variability in muonic production rates reported in the literature (e.g., Heisinger et al., 2002a, b; Braucher et al., 2003, 2011; Phillips et al., 2016), we propagated a 50 % uncertainty on the SLHL muonic production rates. Altitude scaling was based on the 3 arcsec SRTM-4 DEM data set (Jarvis et al., 2008). A topographic correction factor ($F_{\text{topo}}$) from shielding from surrounding topography was applied on a pixel-by-pixel basis for 10° azimuth steps and a 15 km surrounding area following Dunne et al. (1999). Production rates under glacial areas were set to zero ($F_{\text{glacier}}$) using the Global Land Ice Measurements from Space (GLIMS) glacier database (Raup, 2007). Denudation rates were computed from Eq. (1) and production rates estimated from Eq. (2).

The cosmogenic-derived sediment fluxes ($\phi_{\text{cosmo}}$) were computed from the cosmogenic denudation rates following $\phi_{\text{cosmo}} = \varepsilon \times \rho \times S$ (with $\rho$ the density of the eroded material, 2.7 g cm$^{-3}$, and $S$ the basin surfaces). For sediments sampled in rivers downstream of the Himalayan front and having a significant upstream Himalayan drainage, we derived an apparent Himalayan denudation rate by restricting the mean production rate to the Himalayan topography, i.e., by considering the area above 300 m a.s.l. (roughly the floodplain to Siwalik transition) (Lupker et al., 2012). It assumes no sediment addition by incision or significant in situ $^{10}$Be production in the Brahmaputra plain, which is supported by the absence of any trace of significant river incision in the floodplain. Lateral channel migration may nevertheless recycle floodplain sediment but the fluxes are overall supposed to be small and the effect of this recycling only marginally

increases the [10]Be budget of sediments in the floodplain as was suggested for the neighboring Ganga catchment (Lupker et al., 2012).
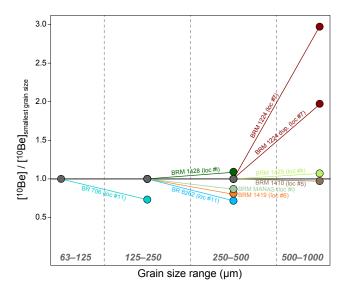
## 3 Results

### 3.1 Occurrence of natural [9]Be

The unrecognized occurrence of [9]Be in addition to the amount of [9]Be introduced by the carrier solution leads to an underestimation of cosmogenic [10]Be concentrations and, hence, to an overestimation of calculated denudation rates. Measured [9]Be concentrations are shown in Table S2 and were put into relation to the amount of [9]Be added to the sample by the carrier solution. Out of the 33 samples, 8 showed significant amounts of natural [9]Be in the quartz samples (i.e., 5 % or more of the [9]Be amount of the carrier) with [9]Be concentrations in quartz reaching up to 1.5 ppm. High [9]Be concentrations were mainly found in samples from three adjacent catchments, tributaries to the Brahmaputra: the Tsang Chhu (pt. m in Fig. 1), the Manas (pt. l), and the Subansiri (pt. j). While we are not aware of any measurement of [9]Be in the quartz from the Manas and the Kameng, the high [9]Be concentrations reported by Portenga et al. (2015) are all from the Tsang Chhu catchment, draining western Bhutan. This suggests that the occurrence of significant [9]Be concentrations in quartz from the Brahmaputra basins is restricted to a few basins on the southern edge of the Tibetan Plateau. Replicate analyses show that for samples with a low [9]Be content, the reproducibility is satisfactory. However, the samples with higher concentrations also show a high variability in their [9]Be content amongst aliquots of the same sample. This suggests that the carrier phase of [9]Be is heterogeneously distributed within the sample and is prone to nugget effects. Accurately correcting for this additional [9]Be contribution therefore proves to be difficult based on the a posteriori measurements of [9]Be in quartz aliquots of the sample. These observations call for the systematic measurement of the [9]Be concentration in an aliquot of the quartz sample that is being used for the AMS [10]Be / [9]Be ratio measurement as suggested by Corbett et al. (2016). For this work, we nevertheless made an attempt to correct for the possible occurrence of [9]Be by propagating conservative uncertainties on the amounts of natural [9]Be that were measured by ICP-MS (Table S1). Given the variability in the replicate [9]Be data (Table S2) we propagated an overall uncertainty of 100 % on the measured [9]Be concentration. In most cases, in which the contribution of natural [9]Be compared to the carrier [9]Be content is small, this additional uncertainty had little effect on the final uncertainty of the [10]Be concentration. It is only significant for samples with high concentrations of natural [9]Be from the Tsang Chhu (pt. m), the Manas (pt. l), and the Subansiri (pt. j) (Table S1). Samples for which no natural [9]Be concentration measurements could be made did not belong to these basins and therefore likely only contain small amounts of [9]Be. We nevertheless conservatively propagated an uncertainty of 2 % on the total amount of [9]Be added to these samples.

### 3.2 [10]Be concentrations, denudation rates, and erosion fluxes

Overall, the [10]Be concentrations measured across the Tsangpo-Brahmaputra span almost 3 orders of magnitude and vary from $1.2 \times 10^6$ to $5 \times 10^3$ at g$^{-1}$. Concentrations are highest in the upper reaches of the Tibetan Plateau and decrease downstream. The lowest [10]Be concentrations are measured for tributaries of the Tsangpo-Brahmaputra that drain the southern and eastern parts of the range (Teesta, Subansiri, Dibang, and Lohit). The [10]Be concentrations were measured in a total of four different grain size fractions (63–125, 125–250, 250–500, 500–1000 μm) to assess possible grain size effects across the Tsangpo-Brahmaputra catchment. Samples only contained enough material for [10]Be measurements in two adjacent grain size fractions at most. The difference in [10]Be concentration across grain size fractions of a single sample remains limited to 30 % (Fig. 2), except for sample BRM1224 (pt. 7) for which the measured 500–1000 μm grain size concentration is a factor of 2 to 3 higher than the finer fraction. The difference in concentration for these two grain size classes is robust since the quartz purification procedure, chemical separation, and AMS measurement has been duplicated but in the absence of any obvious explanation we suggest that this difference might be due to the mixing of sediment from different sources with different grain sizes and [10]Be concentrations. Concentrations measured for the Tsangpo-Brahmaputra River in Bangladesh (pt. 11) also vary within a factor 2 for the seven measurements (five samples) that were performed.

Catchment-wide denudation rates were calculated using Eqs. (1) and (2). The denudation rates measured in the Tsangpo-Brahmaputra basin range from 0.03 to >4 mm yr$^{-1}$ with generally low denudation rates measured on the Tibetan Plateau ($<0.3$ mm yr$^{-1}$). Denudation rates measured along the Tsangpo-Brahmaputra main stream increase downstream of the NBGPm and reach values of ca. 0.5 to 1.5 mm yr$^{-1}$ in the floodplain (floodplain corrected values, i.e., contribution from upstream areas above 300 m a.s.l. only). In Bangladesh, the average denudation rate for the entire Tsangpo-Brahmaputra catchment is $1.0 \pm 0.2$ mm yr$^{-1}$ based on all measurements. The highest measured denudation rates associated with the rivers draining the southern and especially the eastern flanks of the range culminate above 2 mm yr$^{-1}$ for the Lohit and Dibang rivers.

The sediment fluxes that are derived from the denudation rate estimates generally increase downstream along the main stream of the Tsangpo-Brahmaputra and reach $1140 \pm 240$ Mt yr$^{-1}$ at the outlet in Bangladesh. The main increase in sediment fluxes occurs during the transit of the river through the Himalayan range and the NBGPm (locations 3 to

**Figure 2.** Ratio of $^{10}$Be concentrations from grain size pairs of the same sediment sample. Concentrations are normalized to the concentration of the lowest grain size fraction for comparison amongst samples.

8), but the sediment fluxes as measured by $^{10}$Be show only a little increase within the floodplain (locations 8 to 11) despite some significant inputs from tributaries. The main tributaries to the Tsangpo-Brahmaputra in terms of sediment flux are the Yigong and Parlung Zangbo rivers within the syntaxis (combined, ca. 100 Mt yr$^{-1}$) and further downstream the Lohit, Dibang, and Subansiri catchments that export more than 100 Mt yr$^{-1}$ each.

## 4 Discussion

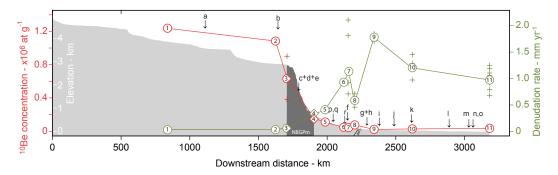### 4.1 Evolution of TCN signals along the Tsangpo-Brahmaputra

#### 4.1.1 Denudation rates lag downstream of the NBGPm

The main trunk river of the Tsangpo-Brahmaputra catchment drains highly contrasted physiographic units with different denudation rates. The NBGPm in particular shows very active erosion processes, with steep river gradients and active landsliding that coincide with rapid exhumation (Finnegan et al., 2008; Stewart et al., 2008; Enkelmann et al., 2011; Larsen and Montgomery, 2012; Lang et al., 2015; King et al., 2016). The NBGPm separates the slowly eroding (< 0.3 mm yr$^{-1}$), high-altitude (> 4000 m) Tibetan Plateau from the lower-lying reaches of the Tsangpo-Brahmaputra (< 2000 m) and the Indo-Gangetic floodplain (< 200 m). The effect of the NBGPm on TCN concentrations is shown in Fig. 3. The $^{10}$Be concentration of sediments sampled along the main stream of the Tsangpo-Brahmaputra decreases by almost an order of magnitude downstream of the NBGPm, highlighting the dilution of high $^{10}$Be concentration Tibetan Plateau sediments by

low-concentration sediments produced in the NBGPm. This decrease in concentration coincides with the river's main knickpoint, which is also the zone of current high erosion rates as documented by the literature.
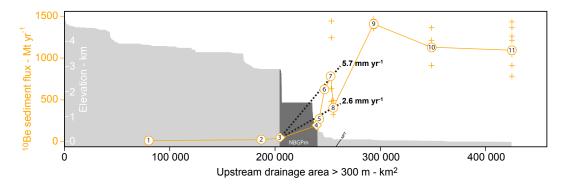
The Tsangpo-Brahmaputra $^{10}$Be CWDR long profile in Fig. 3 shows that the denudation rates rapidly increase (from less than 0.1 mm yr$^{-1}$ before pt. 3 to ca. 1 mm yr$^{-1}$ for pts. 6 to 11) across the eastern Himalayan syntaxis, suggesting the progressive addition of rapidly eroding areas to the total drainage area of the main stream of the Tsangpo-Brahmaputra. However, Fig. 3 also suggests that the main increase in denudation occurs in the syntaxis, between pts. 4 and 7, i.e., about 150 km downstream of the NBGPm area of high exhumation and denudation rates (Finnegan et al., 2008; Stewart et al., 2008; Enkelmann et al., 2011; Larsen and Montgomery, 2012). Catchment-wide denudation rates reach a maximum just before crossing the Main Frontal Thrust (MFT) and exiting the Himalayan range at pt. 8. A similar observation can be drawn from the evolution of the $^{10}$Be-derived sediment flux. The measured sediment fluxes remain low even after crossing the main river knickpoint of the NBGPm with TCN sediment fluxes only increasing significantly after pt. 4. In Fig. 4, $^{10}$Be-derived sediment fluxes are plotted as a function of upstream area. On such a plot, the average denudation rate over a particular river reach is given by the slope between data points. The apparent denudation rate of the NBGPm area, calculated between pts. 3 and 4, equals ca. 1.6 mm yr$^{-1}$. The highest denudation rates however occur further downstream of the NBGPm and peak between pts. 5 and 6 with an apparent denudation rate of 26 mm yr$^{-1}$ and are overall higher than in the NBGPm between pts. 4 and 7 (15 mm yr$^{-1}$). Discrepancies between consecutive upstream and downstream estimates, and especially between pts. 7 and 8, suggest local perturbations of the sediment transport system. The cause of these perturbations remains difficult to explain. Recycling of Siwalik sediments could explain such a trend but the Siwalik-drained area is extremely small (< 100 km$^2$; Acharyya et al., 2007) so that a steady-state Siwalik contribution would be negligible. In addition, our two samples have been sampled 2 years apart from the two opposing banks, which should avoid the sampling of sudden, local, and stochastic Siwalik inputs.

#### 4.1.2 True denudation rates or possible biases in the TCN signal?

The presence of an intensely eroding area in the eastern Himalayan range downstream of the NBGPm, along the lower Siang, down to the MFT, has not been documented by previous studies. Studies suggest that most of the sediment is produced within the NBGPm in both the long and short term. Thermochronological data (Finnegan et al., 2008; Stewart et al., 2008; Bracciali et al., 2016; Salvi et al., 2017) display minimum closure ages for various thermochronometers in a reduced area centered at the confluence between
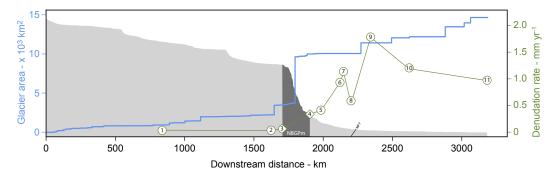
**Figure 3.** Downstream evolution of the [10]Be concentration (red) and corresponding denudation rates (green) of samples from the Tsangpo-Brahmaputra trunk stream. The elevation profile of the trunk stream channel is plotted in shaded grey. Arrows that point down refer to the confluences with the main Tsangpo-Brahmaputra tributaries. Open symbols are based on the average [10]Be concentration of all samples when multiple samples have been analyzed and crosses represent individual measurements. Open circles are from this study and open diamonds are samples from Finnegan et al. (2008).



**Figure 4.** Evolution of the [10]Be-derived sediment flux as a function of the upstream drainage area above 300 m of elevation (in order to remove floodplain area storing sediments) from the Tsangpo-Brahmaputra trunk stream along with the channel elevation profile in grey. The average denudation rate over a given reach of the river is given by the slope of the regression between sample points. Open symbols are based on the average [10]Be concentration of all samples when multiple samples have been analyzed and crosses represent individual measurements. Open circles are from this study and open diamonds are samples from Finnegan et al. (2008).

the Po-Tsangpo and the Yarlung Tsangpo, even though this area with high denudation rates has been suggested to extend farther southwards than earlier recognized (Enkelmann et al., 2011). The recent erosional activity displays a similar pattern, with a maximum landslide density in the NBGPm around the abovementioned confluence, and which significantly decreases further downstream along the upper Siang (Larsen and Montgomery, 2012). Our [10]Be denudation rates do not show any compelling evidence of high denudation along the lower reach of the Siang River. Downstream of the NBGPm, the [10]Be denudation rates from tributaries of the main stream of the lower Siang such as the Siyom River (pt. f) or three other smaller tributaries (pts. p, q, and r) indicate apparent denudation rates of 0.4 to 0.6 mm yr$^{-1}$ in that area, which is much lower than the 4 to 10 mm yr$^{-1}$ suggested by the slope between pts. 4 and 7–8 in Fig. 4. In the absence of other evidence for localized and intense denudation downstream of the NBGPm, we hypothesize that resolving these apparently contradictory results requires consideration of possible biases in the apparent CWDRs along the

Tsangpo-Brahmaputra; several scenarios are therefore explored in the following.

Calculations of CWDR most commonly hypothesize that quartz is ubiquitous. However, nonuniform quartz distributions may yield significant biases in the downstream TCN-derived sediment fluxes (Carretier et al., 2015a). In our case, very low quartz concentrations in the outcropping rocks of the NBGPm might explain the apparent absence of response in the TCB-derived flux signal (Fig. 4). If the Tibetan headwaters partly drain carbonate-rich TSS (Liu and Einsele, 1994) or Linzigong volcanics, the quartz flux exported by the Tibetan Plateau would tend to be overestimated. Nevertheless, if we neglect a thin band of marbles and ophiolites along the highly deformed suture, the metamorphic or igneous, gneissic, and granulitic lithologies outcropping in the NBGPm do not present, to our knowledge, a major difference in quartz amounts compared to the Himalayan metamorphic rocks further south. In addition, such bias would not permit explanation of the very high apparent increase in sediment flux along the lower Siang (Fig. 4).
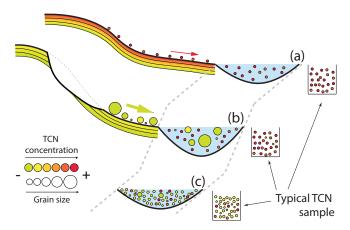
**Figure 5.** Downstream evolution of the total drained glaciated area (GLIMS database; Raup et al., 2007) of the Tsangpo-Brahmaputra in blue. For comparison, the evolution of the trunk channel elevation is plotted in grey and the average $^{10}$Be denudation rate in green.

Another possible source of perturbation of TCN signals in high-altitude environments such as the Himalayas is the input of glacial sediments. Glacially sourced sediments have been shielded from cosmic rays due to the thick ice cover and therefore have low $^{10}$Be concentrations (Godard et al., 2012; Delunel et al., 2014). Figure 5 shows the evolution of the drained glaciated area along the main stream of the Tsangpo-Brahmaputra. The TCN-derived denudation rates increase downstream of the major area of glaciation and the NBGPm. It is therefore unlikely that glacier sediments are the main cause for the observed downstream lag in TCN signals since the glaciated proportion of the catchment is already significant upstream of the main knickpoint (i.e., upstream of the main increase in CWDR) and increases little downstream of it. The main increase in glacial contribution occurs in the NBGPm region, as the Tsangpo receives the contribution of the heavily glaciated Yarlung–Parlung catchments. Glacial contributions would therefore result in a decrease in $^{10}$Be concentrations within the NBGPm rather than further downstream.

Additional processes that may affect TCN signals in steep, highly eroding areas are stochastic events and poor sediment mixing. Landslides and other catastrophic events may perturb the downstream TCN concentration and, hence, bias calculated CWDRs by supplying low-TCN-concentration sediments from previously shielded bedrock (Kober et al., 2012). Modeling studies suggest that this effect is more pronounced for small catchments of a few tens of square kilometers or less and the magnitude of the perturbation depends on the ratio of landslide volume to catchment-averaged sediment flux (Niemi et al., 2005; Yanites et al., 2009). The catchments drained by the Tsangpo-Brahmaputra downstream of the NBGPm exceed 200 000 km$^2$ but these are characterized by a very heterogeneous denudation rate. The riverine TCN signal will be prone to perturbation in the upstream reaches of the syntaxis region, where the upstream sediment flux is still low and the difference in the $^{10}$Be concentration between the sediments carried by the river and landslide material is high. Further downstream of the NBGPm, the effect of landslides should be less important because of the rapidly

increasing river sediment flux and decreasing $^{10}$Be concentration and we therefore expect that regular and diffuse landsliding is likely not a major source of perturbation for CWDRs downstream of the NBGPm. The differences in $^{10}$Be concentrations and CWDR obtained from sediments at pts. 7, 8, and 9 nevertheless suggest that stochastic processes might influence the sedimentary signal. There is no tributary upstream of pt. 8. that could explain the anomalously high local $^{10}$Be concentration (or anomalously low denudation rate). The reasons for this particular perturbation remain unclear but the river reach between the NBGPm and the MFT is prone to extreme hydrological and erosion events (Lang et al., 2011). A recent major perturbation of the sedimentary system was provided by the catastrophic breaching of a landslide-dammed lake on the Yigong River in 2000, which resulted in a devastating flood downstream of the confluence with the Tsangpo-Brahmaputra (Delaney and Evans, 2015). The high discharge that followed the dam breach mobilized about $1 \times 10^8$ m$^3$ or 270 Mt of landslide material in the area (Larsen and Montgomery, 2012). This additional flux of sediments is equivalent to the amount of sediment transported by the Tsangpo in 1 to 3 years depending on the sediment flux estimates. Some remnant sediments of this event are still present in the channel downstream of the breach (Lang et al., 2013). However, over 12 years after this catastrophic flood it is unlikely that these sediments still dominated the sediment budget at the time of sampling, since most of this input has likely been evacuated.

There are no clear geomorphological indications that denudation rates downstream of the NBGPm are actually higher than those in the NBGPm. Evidence for other perturbations of the TCN signal that could explain the lag in denudation rates downstream of the NBGPm such as glacial sediment input, diffuse landsliding, or recent catastrophic flood events are also missing. We therefore explore other processes in the following paragraphs.

**Figure 6.** Conceptual diagram illustrating the evolution of the sediment $^{10}$Be signal in the Tsangpo-Brahmaputra. **(a)** Sediments with a high $^{10}$Be concentration are transferred to the channel in the slowly eroding upstream Tibetan part of the catchment. **(b)** The high-concentration $^{10}$Be flux is diluted by low-concentration sediment produced by landslides within the NBGPm region. However, landslides mainly transfer coarse material to the channel so that the sediments sampled within the sand fraction that is typically used for $^{10}$Be measurements is still dominated by material derived from the Tibetan Plateau. **(c)** Further downstream, abrasion processes transfer sediment from the coarse-grained landslide material into the sand fraction so that the denudation signal of the NBGPm is only sampled downstream of the actual location of intense denudation.

### 4.1.3 Abrasion of landslide material

Abrasion of the sediment load during fluvial transport can affect TCN concentrations because the grain size fraction analyzed is not necessarily representative of the entire sedimentary load (Carretier and Regard, 2011; Lukens et al., 2016). Olen et al. (2015) suggest that abrasion of the sand fraction during transport could affect the TCN signal in some Himalayan rivers when sand grains produced in the headwater regions are abraded during transport and transferred to grain sizes smaller than what is typically analyzed. However, in the case of the Tsangpo-Brahmaputra this would imply that sediments coming from the South Tibetan region would pass below the analyzed grain size fraction and be overwhelmed by low-$^{10}$Be-concentration sandy material from the NBGPm, which is the opposite of what we observe. In addition, once within the sand fraction, abrasion processes are limited by viscous dampening during transport (Jerolmack and Brzinski, 2010) and the downstream fining observed in sand-dominated rivers occurs over very long distances (Frings et al., 2008). Abrasion processes during fluvial transport may also play a role in the TCN concentration evolution of sandy material through the production of sand by pebble attrition. In the case of the NBGPm, landsliding is the main process that produces and transfers sediments to the main channel (Larsen and Montgomery, 2012). Landslides predominantly produce coarse debris (Attal and Lavé, 2006)

and can perturb downstream signals (Kober et al., 2012; West et al., 2014). The large amount of coarse debris delivered to the river is however only reflected in the TCN concentrations of the sand fraction once they are transferred into grain sizes (between 125 and 1000 μm) due to abrasion (Fig. 6). In the case of the NBGPm, we therefore suggest that the upstream TCN signal from the Tibetan Plateau could only be slowly diluted by low-concentration sediments produced in the NBGPm because of the transport distance necessary to transform landslide clasts into sandy material.

To explore the effects of abrasion on the TCN signal in the Tsangpo-Brahmaputra catchment, we constructed a quantitative model of fluvial abrasion that includes the dominant landslide-derived sediment production (Attal and Lavé, 2006). This model allows us to estimate the typical distances over which this dilution is predicted to occur in a setting such as the Tsangpo-Brahmaputra. The model evaluates the response of apparent TCN denudation rates, $\overline{\varepsilon}_{app}$, for a given input sediment flux and TCN concentration that is progressively diluted by the abrasion products of coarse landslide material. Each block or rock fragment, after delivery from the hillslopes to the river network, will be submitted to breaking, crushing, and abrasion, which tend to round the fragment and decrease its diameter. We assume that pebbles >2 mm in diameter are abraded over a distance d$L$ following the commonly used Sternberg's law (Sternberg, 1875), $dV/V = -k\,dL$, with $k$ the pebble abrasion coefficient (in km$^{-1}$), $V$ the pebble volume, and $L$ the position along the channel. The products of abrasion are mostly fine sediments that then transit as a suspended load (Kuenen, 1956) and may be collected for a typical TCN sample (125–1000 μm). In addition to the abrasion coefficient, $k$, the main parameters controlling the delivery and evolution of the sediment load are $f_g$, the initial fraction of landslide-derived material that is delivered to the channel as pebbles and larger clasts; $f_{as}$, the fraction of abrasion products produced within the channel that are transferred from the coarser fraction to a grain size sampled for TCN analyses (typically 125–1000 μm); and $f_{TCN}$, the initial fraction of landslide material directly delivered to channel in the TCN grain size fraction.

The volumetric flux of sediments within the TCN grain size fraction ($Q_{TCN}$) that is transported at a given distance $L$ from the NBGPm (pt. 3) along the channel is given by the sum of (i) TCN-sized sand from the Tibetan Plateau $Q_{T,TCN}$; (ii) abrasion of bed load delivered from the Tibetan Plateau $Q_{T,b}$; (iii) direct delivery of TCN-sized sand from landslides within the highly eroding areas; and (iv) the abrasion of
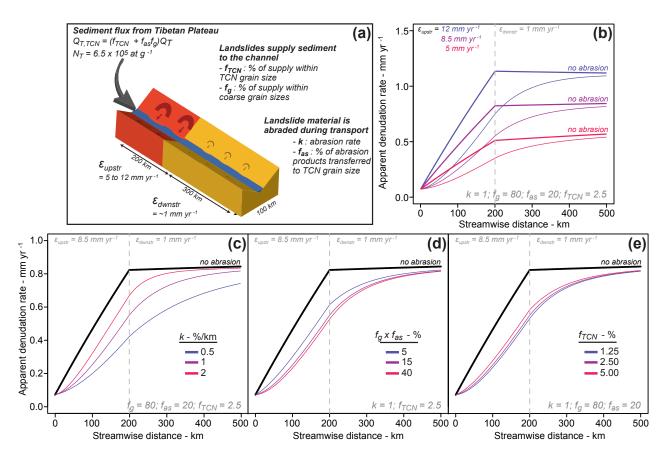
**Figure 7. (a)** Schematic of the modeled river reach: main boundary conditions and process parameters used in the model. Panels **(b)** to **(e)** are abrasion model results showing the apparent $^{10}$Be denudation rate reconstructed from river sediments within the sand fraction in case of abrasion compared to the no-abrasion case (thick line). The sensitivity to changes in different parameters has been explored: **(b)** sensitivity to changes in absolute erosion rates over the modeled reach, **(c)** sensitivity to changes in the abrasion rate coefficient $k$, **(d)** sensitivity to changes in the product between the initial fraction of coarse material ($>2\,\text{mm}$) delivered to the channel $f_g$ and the fraction of this coarse material that is ultimately transferred to the TCN sampled and measured fraction $f_{as}$, and **(e)** sensitivity to changes in the initial fraction of sediment delivered by landslides directly within the TCN grain size fraction $f_{TCN}$. More information on the model setup and results can be found in the text.

coarse landslide material. Therefore,

$$
\begin{aligned}
Q_{\text{TCN}}(L) = {} & Q_{T,\text{TCN}} + Q_{T,b} f_{as} \left(1 - e^{-kL}\right) \\
& + f_{\text{TCN}} \int_0^L w(x)\varepsilon(x)\mathrm{d}x \\
& + f_g f_{as} \int_0^L w(x)\varepsilon(x) \left[1 - e^{-k(L-x)}\right]\mathrm{d}x,
\end{aligned}
\tag{3}
$$

in which $w(x)$ is the local catchment width and $\varepsilon(x)$ is the local denudation rate.

The average TCN concentration of sediments along the main channel, $N(L)$, is then expressed as

$$
N(L) = \frac{N_T\left[Q_{T,\text{TCN}}+Q_{T,b}f_{as}\left(1-e^{-kL}\right)\right]+f_{\text{TCN}}\int_0^L N(x)w(x)\varepsilon(x)\mathrm{d}x}{Q_{T,\text{TCN}}+Q_{T,b}f_{as}\left(1-e^{-kL}\right)+f_{\text{TCN}}\int_0^L w(x)\varepsilon(x)\mathrm{d}x} \\ \frac{+f_g f_{as}\int_0^L N(x)w(x)\varepsilon(x)\left[1-e^{-k(L-x)}\right]\mathrm{d}x}{+f_g f_{as}\int_0^L w(x)\varepsilon(x)\left[1-e^{-k(L-x)}\right]\mathrm{d}x}.
\tag{4}
$$

In steady state, the sediment TCN concentration is related to denudation through Eq. (1), so that Eq. (4) can be rewritten

as

$$N(L) =$$

$$\frac{N_T\left[Q_{T,\text{TCN}}+Q_{T,b}f_{\text{as}}(1-e^{-kL})\right]+f_{\text{TCN}}\int_0^L\sum_i\dfrac{P_i(x)}{\mu_i}w(x)\,\mathrm{d}x}{\begin{array}{c}+f_g f_{\text{as}}\int_0^L\sum_i\dfrac{P_i(x)}{\mu_i}w(x)[1-e^{-k(L-x)}]\mathrm{d}x\\\hline Q_{T,\text{TCN}}+Q_{T,b}f_{\text{as}}(1-e^{-kL})+f_{\text{TCN}}\int_0^L w(x)\varepsilon(x)\mathrm{d}x\\+f_g f_{\text{as}}\int_0^L w(x)\varepsilon(x)[1-e^{-k(L-x)}]\mathrm{d}x\end{array}} . \quad (5)$$

It is reasonable to assume that the upstream coarse bed load sediment flux is limited because of slow denudation rates and long travel distances that allow efficient abrasion and possible sediment trapping on the Tibetan Plateau. This is supported by the valley infill upstream of the gorges being dominated by sands over the upper 100 to 200 m (Wang et al., 2014). Equation (5) simplifies to

$$N(L) =$$

$$\frac{N_T Q_{T,\text{TCN}}+f_{\text{TCN}}\int_0^L\sum_i\dfrac{P_i(x)}{\mu_i}w(x)\,\mathrm{d}x+f_g f_{\text{as}}\int_0^L\sum_i\dfrac{P_i(x)}{\mu_i}w(x)[1-e^{-k(L-x)}]\mathrm{d}x}{Q_{T,\text{TCN}}+f_{\text{TCN}}\int_0^L w(x)\varepsilon(x)\mathrm{d}x+f_g f_{\text{as}}\int_0^L w(x)\varepsilon(x)[1-e^{-k(L-x)}]\mathrm{d}x} . \quad (6)$$

The TCN concentration can then be converted to an apparent denudation rate using Eq. (1) applied to the whole drainage area, including the South Tibetan part:

$$\overline{\varepsilon}_{\text{app}} = \frac{1}{N(L)} \times \sum_i \frac{\overline{P_i}(L)}{\mu_i} = \frac{1}{N(L)}$$

$$\times \frac{1}{S} \int_{\substack{\text{upper} \\ \text{drainage}}} \sum_i \frac{\overline{P_i}(x)}{\mu_i} w(x)\,\mathrm{d}x . \quad (7)$$
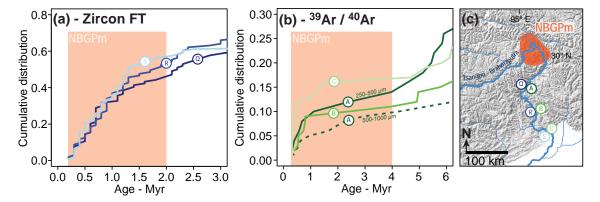
In order to test this abrasion model, the river section downstream of the Tibetan Plateau is simplified to a 500 km long reach with a constant width of 100 km, yielding a total catchment area similar to that of the actual catchment between pts. 3 and 8 (Fig. 7a). The [10]Be production rates in our model are also set to values similar to the average production rates modeled for the Tsangpo-Brahmaputra between pts. 3 and 8 (neutron and muon production scaling factors of 12.7 and 4.4, respectively). Sediment is delivered from upstream with a [10]Be concentration of ca. $6.5 \times 10^5$ at g$^{-1}$ and a total flux of 40 Mt yr$^{-1}$, similar to the sediment flux delivered by the Tibetan Plateau (based on the average concentration at pt. 3). The fraction of this flux within the TCN grain size assumes that all coarse material has been abraded: $Q_{T,\text{TCN}} = \left(f_{\text{TCN}} + f_g f_{\text{as}}\right)Q_T$. The 500 km reach is further subdivided into a 200 km long upstream area with high denudation rates, $\varepsilon_{\text{upstr}}$, representing the supposedly rapid exhumation and erosion NBGPm area followed by a 300 km long lower catchment with lower denudation rates $\varepsilon_{\text{dwnstr}}$. Different pairs of denudation rates can be chosen but if $\varepsilon_{\text{dwnstr}}$ is set to a typical background Himalayan denudation rate of ca. 1 mm yr$^{-1}$

(Lupker et al., 2012), $\varepsilon_{\text{upstr}}$ needs to be between ca. 5 and 12 mm yr$^{-1}$ to satisfy the actual measured downstream [10]Be concentration (ca. $3.9$–$7.8 \times 10^4$ at g$^{-1}$). The range of abrasion parameters $k$, $f_g$, $f_a$, and $f_{\text{TCN}}$ is estimated from abrasion experiments and grain size determinations of landslide material (Attal and Lavé, 2006, 2009; Nibourel et al., 2015).

Figure 7 shows the apparent [10]Be denudation rate in the case of abrasion and for a range of model parameters in comparison to the no-abrasion case. These model results show that for the range of parameters considered there is a downstream spatial lag between the actual denudation rates (no-abrasion case) and the denudation rates determined by the [10]Be concentrations of sediments found in the main channel. The magnitude of this lag is dependent on chosen parameters but ranges from ca. 50 to 150 km. This abrasion model is sensitive to the magnitude of denudation rates in the rapidly eroding part ($\varepsilon_{\text{upstr}}$, Fig. 7b) and, in the case of low denudation rates in the Tsangpo, it is unlikely to be detected because the difference between the denudation rates reconstructed for the abrasion and non-abrasion cases are very similar. The magnitude of the lag is also dependent on the chosen abrasion coefficient, $k$. As $k$ increases, the transfer of mass from the low-concentration landslide material to the analyzed grain size is more rapid and, hence, the dilution of high-concentration upstream sediments occurs earlier along the river reach. However, Fig. 7 also shows that the downstream lag is not sensitive to changes in $f_{\text{TCN}}$, $f_g$, or $f_{\text{as}}$.

These model results suggest that abrasion of landslide material is able to induce a downstream lag in the denudation rate calculated from [10]Be concentration in the sand fraction. The magnitude of the modeled offset is within the range of the observed offset between the supposedly high-denudation-rate area within the NBGPm and the maximum denudation measured occurring about 150 km further downstream. However, our model only takes into account abrasion along the main stream of the Tsangpo-Brahmaputra and does not take into account the abrasion of landslide material that may have occurred in smaller tributaries before reaching the trunk stream. Our model may therefore slightly overestimate the role of abrasion in generating the observed downstream lag in the denudation signal. Testing the limits of this model and directly comparing them to the data in the eastern syntaxis would require the spatial distribution of landslides and drainage area to be modeled explicitly, which is beyond the scope of this contribution.

Conversely, the absence of a relation between grain size and [10]Be denudation rate within the sand size fraction (Fig. 2) might seem at odds with our argument that abrasion processes play an important role in the transfer of the erosional signal from hillslopes to river sediments. Predicting a relation between grain size and TCN concentration on the scale of the whole catchment requires grain size distributions to be quantified for landslide and abrasion products over a large range of climatic, lithologic, and tectonic settings. For the moment, the absence of database or theoretical models

**Figure 8. (a)** Zircon fission track (Enkelmann et al., 2011) and **(b)** $^{39}$Ar / $^{40}$Ar (Lang et al., 2016) of sediment samples from the Tsangpo-Brahmaputra downstream to the NBGPm **(c)** (trimmed to the younger part of the sample age spectrum).

of these processes prevents detailed exploration of the sand size issue. Our simplified model could actually only be validated or invalidated by comparing $^{10}$Be concentration across a large range of grain sizes, i.e., between sand size content and boulder size similar to what has been done by Puchol et al. (2014) and Carretier et al. (2015b), who found lower $^{10}$Be concentrations in pebble-sized sediments.

Abrasion effects in the Tsangpo-Brahmaputra are unlikely to be restricted to detrital TCN studies. Other detrital proxies such as thermochronological ages of sediment grains could be affected similarly, i.e., the young cooling ages found in the NBGPm (e.g., Zeitler et al., 2014) could be transferred to the typically studied sand fraction of the sediment load further downstream only after coarse landslide material is abraded. The population of zircon fission track (FT) ages (Enkelmann et al., 2011) and $^{39}$Ar / $^{40}$Ar ages (Lang et al., 2016) was measured in three Tsangpo-Brahmaputra river sediment samples from downstream of the NBGPm to the Himalayan front (Fig. 8). In both cases, the relative proportion of the youngest grains (< 2 Myr for zircon FT and < 4 Myr for $^{39}$Ar / $^{40}$Ar) does not significantly decrease downstream of the NBGPm (based on a two-sample, one-sided, Kolmogorov–Smirnov test at the $p = 0.1$ level) as would be expected if the NBGPm signal were diluted by sediments from lower exhuming areas. While the zircon FT populations of the three samples are not significantly different, the $^{39}$Ar / $^{40}$Ar data show that the proportion of young grains increases from A to C ($p = 0.1$). This later observation is expected if the NBGPm rapid exhumation signal is transferred to the sand fraction only after abrasion of the coarse NBGPm landslide material. More samples are obviously needed to further test this hypothesis but we speculate that similar abrasion should be considered in actively eroding areas for a range of detrital sediment provenance and denudation tracers.

## 4.2 Denudation budget of the Tsangpo-Brahmaputra

### 4.2.1 Denudation of the upstream Tibetan Plateau part of the Tsangpo-Brahmaputra catchment

Denudation rates measured upstream of the NBGPm and on the Tibetan Plateau are the lowest denudation rates measured in the Tsangpo-Brahmaputra catchment (ca. 0.04 to 0.2 mm yr$^{-1}$). These low denudation rates are of the same order of magnitude as previously published bedrock and detrital denudation rates in other areas of the plateau (Lal et al., 2004; Kong et al., 2007; Hetzel et al., 2011; Strobl et al., 2012; Li et al., 2014; Rades et al., 2015). The slightly higher denudation rates measured for the two northern tributaries, the Lhasa-He (Kyi) (pt. a) and Nyang (pt. b) (0.08 and 0.2 mm yr$^{-1}$, respectively), are associated with higher catchment-averaged relief and slopes (Table S1). Duplicate measurements from samples taken 4 years apart (this study and Finnegan et al., 2008) show reproducible denudation rates for the Nyang (pt. b), but vary by a factor of 2 for the main stream of the Brahmaputra-Tsangpo at pt. 3. This later variability could be associated with the stochasticity of the sediment transport system that does not always result in a perfectly mixed sample. It should however be noted that sample TSA-16 yields a sediment flux of ca. 30 Mt yr$^{-1}$ that is compatible with the upstream mass balance (Tsangpo-Brahmaputra at pt. 2 with 20 Mt yr$^{-1}$ and the Nyang with 10 Mt yr$^{-1}$), while NB-8-04 potentially overestimates this mass balance (with a flux at pt. 3 of 70 Mt yr$^{-1}$). Overall, the $^{10}$Be data added by this study highlight the relative landscape stability of the upper part of the Tsangpo-Brahmaputra catchment in comparison to the Tibetan Plateau margins. It also suggests that the sediment supply from the upper reaches of the Tsangpo-Brahmaputra is limited compared to its downstream drained area.
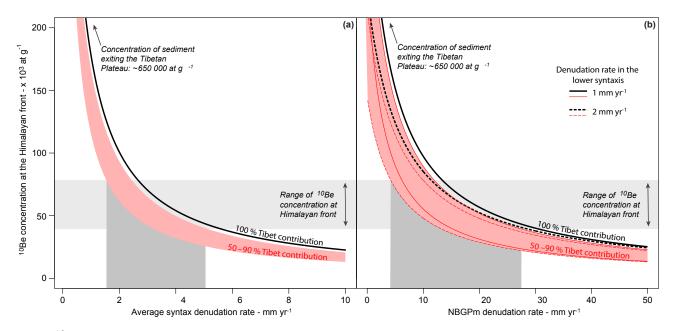
**Figure 9.** $^{10}$Be concentration mixing model. **(a)** The concentration of sediments exported at the Himalayan front (pts. 7–8) is calculated by mixing sediments from the Tibetan Plateau (pt. 3) with sediments produced along the entire syntaxis (pts. 3 and 7–8) for a range of denudation rates in the syntax. **(b)** The mixing model is calculated for variable denudation rates within the restricted area of the NBGPm, mixing with sediments exported by the Tibetan Plateau, tributaries within the syntaxis (pts. c, d, e) as well as for two estimates of denudation rates in the lower part of the syntaxis (1 and 2 mm yr$^{-1}$). The $^{10}$Be concentration modeled at the Himalayan front is then compared to the $^{10}$Be concentrations actually measured (pts. 7–8) in order to constrain the range of possible denudation rates in the entire syntaxis **(a)** and the NBGPm **(b)**. The solid and dashed black curves are the modeled concentrations assuming that 100 % of the sediment flux predicted by the TCN is exported by the Tibetan part of the catchment. However, as discussed in the text, sediment storage and lower quartz abundances imply fluxes that are likely only 50 to 90 % of the TCN-derived flux. The model results for a reduced Tibetan contribution are shown by the red shaded area and result in lower denudation rate estimates for the entire syntaxis (**a** 1.8 to 5.1 m yr$^{-1}$) and the NBGPm (**b** 4 to 27 mm yr$^{-1}$).

## 4.2.2 Denudation of the eastern syntaxis and of the NBGPm

Denudation rates downstream of the Tibetan Plateau, from the NBGPm to the MFT (i.e., the Himalayan part of the Tsangpo-Brahmaputra main stream course), need to be considered carefully because of the abrasion processes discussed above. Endorsing this model of downstream lag in the TCN response due to abrasion effects means that the samples along the main stream of the Tsangpo-Brahmaputra cannot be used to provide tight spatial constraints on the location and magnitude of denudation within the NBGPm. The denudation signal is not immediately transferred to the TCN grain size in the trunk stream and hence TCN samples do not accurately represent the upstream denudation processes. A first-order estimate of the denudation rates in the eastern Himalayan part of the Tsangpo-Brahmaputra can nevertheless be made by assuming that the onset of the steep gorges and the knickpoint marks the onset of intense landsliding (Larsen and Montgomery, 2012) and that abrasion processes become less significant beyond the gravel–sand transition at the Himalayan front (Dubille and Lavé, 2015) close to the MFT. The evolution of the $^{10}$Be-derived sediment fluxes as a function of upstream area (Fig. 4) constrains the average denuda-

tion to be within ca. 2.6 to 5.7 mm yr$^{-1}$ for that part of the catchment by using the average $^{10}$Be-derived sediment flux of pt. 3 at the gorge entrance and pts. 7 or 8 at the downstream end (calculated using the average concentration at each point).

A very similar estimate can be made by estimating the $^{10}$Be concentration and flux of sediments produced in the syntaxis region that is required to dilute the upstream signal to the levels measured downstream of the syntaxis. Such a $^{10}$Be mixing model is shown in Fig. 9a: the $^{10}$Be concentration of sediments exported at the outlet of the Himalayan front (pt. 8) is calculated by mixing sediments fed by the Tibetan part of the catchment (above pt. 3: 650 000 at g$^{-1}$) with sediments produced within the entire syntaxis for a range of denudation rates (for neutron and muon production scaling factors of 12.7 and 4.4, respectively). The $^{10}$Be concentration of downstream sediments that exit the syntaxis should fall within the actual range of measured $^{10}$Be concentrations to be compatible with our data (3.9–7.8 × 10$^4$ at g$^{-1}$) and allows us to constrain the average denudation rates within the entire syntaxis. However, thermochronological data (e.g., Enkelmann et al., 2011; Salvi et al., 2017), river gradients (Finnegan et al., 2008), and landslide density (Larsen and Montgomery, 2012) argue for nonuniform denudation in the
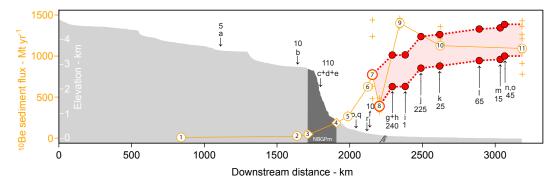
**Figure 10.** Evolution of the $^{10}$Be-derived sediment flux as a function of distance along the Tsangpo-Brahmaputra trunk stream along with the channel elevation profile in grey. The arrows show the addition of sediments from tributaries along with their $^{10}$Be-derived sediment addition in megatons per year. The red curves show the evolution of the total sediment flux that is obtained by adding the $^{10}$Be-derived sediment flux of tributaries **(g–o)** to the Tsangpo-Brahmaputra sediment flux measured at the front of the Himalayan range (with a flux of 770 Mt yr$^{-1}$ at pt. 7 or 390 Mt yr$^{-1}$ at pt. 8). The sediment flux at pts. 10 and 11 is compatible with the addition of sediment from tributaries (i.e., within the range of the red curve); the sediment flux measured at pt. 9 exceeds these estimates.

eastern syntaxis with focused erosion in the NBGPm. A second estimate can therefore be made by assuming that the high denudation rate in the NBGPm is restrained to ca. 5000 km$^2$ (Larsen and Montgomery, 2012). Using a similar mixing approach as explained above, we calculated the $^{10}$Be concentration of sediments at the Himalayan outlet that results from the mixing of (a) sediments shed by the Tibetan Plateau part of the catchment; (b) sediments from the NBGPm (with neutron and muon production scaling factors of 9.1 and 3.6, respectively) experiencing variable denudation rates ranging from 0 to 50 mm yr$^{-1}$; (c) sediment contributions based on the available $^{10}$Be data from the Rong Chu, Yigong, and Parlung rivers (pts. c, d, and e; 130 Mt yr$^{-1}$ with a flux-weighted average $^{10}$Be concentration of $2.1 \times 10^4$ at g$^{-1}$); and (d) sediment contributions from the lower part of the syntaxis (downstream of the NBGPm) where we assume typical Himalayan denudation rates of 1 to 2 mm yr$^{-1}$. This model shows that the denudation rate within the NBGPm needs to be between ca. 12 and 31 mm yr$^{-1}$ to match the actual $^{10}$Be concentration measured at the outlet of the Himalayan front (solid and dashed curve in Fig. 9b). This latter estimate is obviously dependent on the denudation rate attributed to the downstream part of the reach, which has not been systematically constrained in this study. Our samples from small tributaries of the Tsangpo-Brahmaputra suggest denudation rates as low as 0.4 to 0.6 mm yr$^{-1}$ (pts. p, q, r, and f in Fig. 1). Thermochronological data also suggest exhumation rates significantly lower than the NBGPm (Salvi et al., 2017), suggesting overall low denudation rates.

One important underlying assumption for these denudation rate estimates is that the entire upper Tibetan part of the catchment is connected to the Tsangpo-Brahmaputra trunk stream and that its entire drainage area exports sediments at the calculated rate. A number of observations tend to suggest that this may not be the case. The upper Tsangpo is partially dammed along its course by several active and potentially subsiding N–S horst and graben systems (Armijo et al., 1986), and several hundred meters of Quaternary sediments are also stored directly upstream of the Tsangpo Gorge (Wang et al., 2015). Internally drained areas and lakes represent additional breaks in the sediment cascade. Furthermore, the Tibetan headwaters drain the carbonate-rich TSS (Liu and Einsele, 1994), which contain lower amounts of quartz than the Himalayan or NBGPm metamorphic rocks. This would tend to overestimate the quartz flux that is exported by the Tibetan Plateau relative to the quartz fluxes eroded downstream. In both cases, the actual sediment flux exported by the South Tibetan part of the catchment may be overestimated if calculated directly using $^{10}$Be denudation rates and total catchment area. Constraining the magnitude of this overestimation requires an independent estimate of the sediment flux at the range outlet. Goswami et al. (1985) reported a sediment flux of ca. 210 Mt yr$^{-1}$ in Pasighat (pt. 8), which is only 30 to 55 % of the sediment flux estimated from the $^{10}$Be data at the range outlet and which would correspond to a Tibetan Plateau contribution reduced to only 15 to 40 % of the reference flux. However, the sediment gauging details and method of this flux estimate remain undocumented, and the timescale covered by these gauging data is significantly lower than that of the TCN estimates. The TCN mass balance, just upstream of the eastern syntaxis between the Yarlung Tsangpo and the Nyang rivers, which is unaffected by sediment sequestration in grabens or contrasted quartz contents, is also not very conclusive: the TCN concentration of sample TSA-16 below the confluence of these two rivers (pt. 3) requires mixing Nyang sediment (pt. b) with 100 % of $^{10}$Be-derived (pt. 2) Yarlung Tsangpo sediment flux (pt. 2), whereas the sample NB-8-04 rather suggests an upper Tsangpo contribution limited to 20 % of the $^{10}$Be-derived sediment flux. Conversely, direct estimation of

the average sedimentation in Yarlung Tsangpo buried canyon (Wang et al., 2015) over the last 2 Myr suggests that the sequestration flux there was limited to ∼ 1 %. A similar calculation for the grabens crossed by the Yarlung Tsangpo further west is not possible due to limited data on subsidence rates: a priori late Cenozoic low slip rates ($< 1 \, \text{mm yr}^{-1}$) on the nearby Kung Co half graben (Mahéo et al., 2007) would suggest a moderate sequestration of a few percent of the total sediment flux. Furthermore, the modest decrease in TCN concentration between pts. 1 and 2 (Fig. 1) also tends to suggest that sediment sequestration between these points is limited because otherwise we would expect the TCN concentration in the main stream to be more significantly lowered by the lower-[10]Be-concentration sediment input from the Lhasa-He (pt. a). Finally, the mineralogical composition of the upper Tsangpo-Brahmaputra sediments suggests a lower proportion of quartz grains compared to those of the Tsangpo-Brahmaputra River close to the outlet, but this deficit lies between 15 and 35 % (Garzanti et al., 2004).

Altogether, we therefore suspect the sediment entering into the eastern syntaxis at pt. (3) to be lower than the actual flux predicted by the TCN, but we think that this difference remains relatively small. We conservatively speculate here that the actual flux exported by the Tibetan Plateau part of the catchment ranges between 50 and 90 % of the flux that would be calculated by the TCN. The exact magnitude of this sediment flux reduction remains to be quantified. Using a similar mixing and dilution model as exposed above, we estimated the effect of a sediment flux exported by the Tibetan Plateau of the catchment that is lower by 50 to 90 % compared to the predicted flux (i.e., a sediment flux of 20 to 36 $\text{Mt yr}^{-1}$; red shaded area in Fig. 9a and b). Lowering the upstream sediment flux greatly reduces the denudation rate estimate within the eastern syntaxis and the NBGPm (Fig. 9). The denudation estimates, using a reduced Tibetan contribution, range from ca. 2 to 5 $\text{mm yr}^{-1}$ for the average denudation rate estimated over the entire syntaxis (pts. 3–8) and 4 to 28 $\text{mm yr}^{-1}$ for the NBGPm (Fig. 9). This later estimate lies at the higher end of the previous estimates of denudation in the NBGPm, which range between 5 and 17 $\text{mm yr}^{-1}$ (Stewart et al., 2008; Enkelmann et al., 2011; Larsen and Montgomery, 2012). These denudation rate estimates are also all significantly higher than other [10]Be denudation rates reported for other Himalayan catchments (Vance et al., 2003; Wobus et al., 2005; Finnegan et al., 2008; Lupker et al., 2012; Godard et al., 2012, 2014; Puchol et al., 2014; Scherler et al., 2014; Le-Roux-Mallouf et al., 2015; Portenga et al., 2015; Morell et al., 2015; Olen et al., 2015, 2016; Abrahami et al., 2016), highlighting the significance of the NBGPm as a denudational hot spot.

### 4.2.3 Downstream denudation of the Tsangpo-Brahmaputra catchment and other Himalayan tributaries

Downstream of the MFT, the Tsangpo-Brahmaputra enters the low-gradient Indo-Gangetic flood plain and receives sediment from a number of significant Himalayan tributaries with denudation rates ranging from 0.7 up to 4 $\text{mm yr}^{-1}$. Three main tributaries dominate the sediment input: the Dibang, Lohit, and Subansiri (pts. g, h, and j in Fig. 1, respectively). To our knowledge, no direct gauging data are available for these rivers, but a significant input from the eastern rivers (chiefly Lohit and Dibang) has been suggested by the geochemical and mineralogical fingerprinting of sediments in the Tsangpo-Brahmaputra main stream (Singh and France-Lanord, 2002; Garzanti et al., 2004). The Lohit and Dibang catchments are characterized by steep slopes and high relief (Table S1). Furthermore, these catchments receive intense rainfall, in excess of 2 m during the Indian summer monsoon according to remote sensing data (Anders et al., 2006; Bookhagen et al., 2006). GPS data further suggest rapid convergence across the south-east to north-west trending Mishmi and Lohit thrusts (Gupta et al., 2015). The interactions between climate and tectonics in the Lohit and Dibang catchments may therefore be translated into high denudation rates and sediment fluxes. The denudation rates in these catchments have likely been underestimated in the past. The high denudation rates measured in the Subansiri are more difficult to explain, especially since its neighboring catchments of the Syom (pt. f), the Kameng (pt. k), and the Manas (pt. l) show significantly lower denudation rates for similar catchment average relief and slope (Table S1), closer to denudation rates found elsewhere for large catchments of the Himalayas (Lupker et al., 2012). The Bhuri Dihing River is the only southern tributary to the Tsangpo-Brahmaputra for which denudation rates have been measured in this work. The Bhuri Dihing drains the northern part of the Indo-Burmese ranges and denudes at a lower rate (0.2 $\text{mm yr}^{-1}$) compared to the main Himalayan tributaries. Denudation rates of the actively uplifting Shillong Plateau have recently been suggested to be very low on average (Rosenkranz et al., 2016).

Overall, according to our TCN data, the Tsangpo-Brahmaputra receives ca. 600 $\text{Mt yr}^{-1}$ of sediments from its tributaries in the Indo-Gangetic floodplain downstream of the MFT. Figure 10 shows the evolution of the sediment flux predicted for the Tsangpo-Brahmaputra by the successive addition of sediment from all its tributaries in the floodplain. Such an approach is only possible for the downstream part of the catchment as our [10]Be data cover all major tributaries of the Tsangpo-Brahmaputra and no significant sediment contribution is considered to come from the floodplain area itself. The predicted flux at the outlet in Bangladesh ranges from 1000 to 1400 $\text{Mt yr}^{-1}$ depending on the sediment flux that is considered to enter the floodplain at the MFT (flux estimate of pts. 7 or 8). Figure 10 shows that the sediment fluxes

and denudation rates measured at the outlet in Bangladesh (pt. 11) and in Tezpur in India (pt. 10) are consistent within uncertainty with the simple addition of sediments from the Tsangpo-Brahmaputra. However, the flux predicted at pt. 9 clearly exceeds what can be expected by the sole addition of sediments from the Lohit and Dibang to the sediment load shed by the Tsangpo-Brahmaputra at the MFT (pts. 7 or 8). The $^{10}$Be concentrations measured at pt. 9 may, therefore, be affected by transient perturbations in the sediment load or poor mixing of upstream contributions and may not be representative of the average sediment load transported by the Tsangpo-Brahmaputra. Repeated sampling at this location would provide better constraints on the variability in the signal at that location.

$^{10}$Be denudation rates measured in Bangladesh at the outlet of the Tsangpo-Brahmaputra catchment (pt. 11) vary between 0.7 and 1.2 mm yr$^{-1}$ for samples that have been collected over 4 different years. This variability is higher than the variability observed for the neighboring Ganga River (Lupker et al., 2012), which suggests that the Tsangpo-Brahmaputra floodplain may be less efficient at smoothing the variability in the upstream TCN signal. The absolute $^{10}$Be sediment fluxes (780–1430 Mt yr$^{-1}$, calculated for a catchment above 300 m elevation) are higher by a factor of 1.5 to 2.5 compared to the gauging sediment flux estimates of 500 and 610 Mt yr$^{-1}$ (Delft Hydraulics, 1996). A similar overestimation, although of lower magnitude, was observed for the Ganga catchment (Lupker et al., 2012). A number of factors may affect this comparison: first, the yearly to decadal integration time of gauged fluxes may not be directly compared to the centennial to millennial fluxes estimated from TCN (Wittmann and von Blanckenburg, 2016); second, the subsiding Indo-Gangetic floodplain may be a significant sediment sink, lowering the actual sediment flux exported to the Bay of Bengal; and third, the overestimation of the contributing Tibetan area will also lead to an overestimation of the $^{10}$Be sediment flux estimates at the outlet by affecting sediment contribution area and catchment-averaged production rates. The respective contribution of these effects remains difficult to quantify and would warrant a more in-depth study, but they need to be considered before directly comparing $^{10}$Be and gauged sediment fluxes in large-scale catchments.

## 5   Conclusions

The $^{10}$Be concentration of sediments carried by the Tsangpo-Brahmaputra are marked by a sharp decrease over the course of the river. High $^{10}$Be concentrations, indicative of low denudation rates on the Tibetan Plateau, decrease by almost an order of magnitude as the river crosses the Namche Barwa–Gyala Peri massif. This observation is compatible with the addition of large amounts of low-$^{10}$Be-concentration sediment in this region with documented high exhumation rates and active landsliding. However, we find that the dilution

of the $^{10}$Be signal occurs only about 150 km downstream of the NBGPm. A possible explanation for this downstream lag in response to high denudation is the role of abrasion processes of predominantly coarse material that is delivered by landslides within the NBGPm. High-concentration sediment exported by the Tibetan Plateau is only diluted by low-concentration landslide material when abrasion reduces the grain size of landslide material to a size that falls within the fraction that is typically analyzed for cosmogenic nuclides. We modeled the effect of abrasion of landslide material on cosmogenic nuclide denudation rates using an idealized reach with characteristics similar to the Tsangpo-Brahmaputra and literature-derived abrasion parameters. This model is able to reproduce a downstream lag in the increase of $^{10}$Be-derived denudation rates ranging between 50 and 150 km and is therefore compatible with our data. Therefore, we propose that dominant hillslope erosion from landsliding combined with delayed sand production from pebble abrasion might significantly bias TCN-derived denudation rates as commonly measured in the sandy fraction of alluvial sediment load. The effect of fluvial abrasion of landslide material may operate in a large number of actively eroding settings, where landslide is a major sediment production process. Its effect on TCN may be substantial and needs to be taken into account, thereby adding to the limitations of the use of TCN in landslide-dominated landscapes, independent of catchment size. These abrasion effects are also very likely transposable to other detrital sediment studies operationally focused on sand-sized sediments and need to be taken into account for provenance, thermochronological, and TCN studies alike.

Our data also provide new constraints on the denudation across the Tsangpo-Brahmaputra catchment. The upstream Tibetan Plateau part of the catchment is denuding at a slow rate inferior to 0.2 mm yr$^{-1}$. The observed downstream lag in the denudation signal of the NBGPm means that the denudation rates within that area cannot be reconstructed at a high spatial resolution. However, we show that it is still possible to use the $^{10}$Be concentrations of samples collected along the main stream of the Tsangpo-Brahmaputra to derive denudation estimates in the eastern Himalayan syntaxis and the NBGPm. The estimate of these denudation rates is, however, affected by the actual sediment flux exported by the Tibetan Plateau of the catchment. Sediment sequestration, disconnected parts of the catchment, and lower quartz content of this Tibetan part will lead to the overestimation of downstream denudation rate estimates. Taking into account these effects, we estimate that the denudation rates over the entire syntaxis are between ca. 2 and 5 mm yr$^{-1}$. If this denudation is mostly attributed to the rapid denudation rate in the restricted area with rapid exhumation and active landsliding, our $^{10}$Be data suggest denudation rates of 4 to 28 mm yr$^{-1}$. Our data therefore confirm the intense denudation rates in the eastern Himalayan syntaxis region in comparison with other estimates across the Himalayan range. We also show the im-

portance of taking into account upstream sediment processes to derive robust estimates. Finally, the denudation rates of the Tsangpo-Brahmaputra in the downstream floodplain part of the catchment are mostly compatible with the addition of fluxes from the Himalayan tributaries. In addition, sediments from the outlet in Bangladesh constrain the average denudation rate of the entire Tsangpo-Brahmaputra to be within 0.7 to 1.2 mm yr$^{-1}$.

**Data availability.** No data sets were used in this article.

**The Supplement related to this article is available online at https://doi.org/10.5194/esurf-5-429-2017-supplement.**

## References

Abrahami, R., van der Beek, P., Huyghe, P., Hardwick, E., and Carcaillet, J.: Decoupling of long-term exhumation and short-term erosion rates in the Sikkim Himalaya, Earth Planet. Sc. Lett., 433, 76–88, https://doi.org/10.1016/j.epsl.2015.10.039, 2016.

Acharyya, S. K.: Evolution of the Himalayan Paleogene foreland basin, influence of its litho-packet on the formation of thrust-related domes and windows in the Eastern Himalayas – A review, J. Asian Earth Sci., 31, 1–17, 2007.

Aguilar, G., Carretier, S., Regard, V., Vassallo, R., Riquelme, R., and Martinod, J.: Grain size-dependent [10]Be concentrations in alluvial stream sediment of the Huasco Valley, a semi-arid Andes region, Quat. Geochronol., 19, 163–172, https://doi.org/10.1016/j.quageo.2013.01.011, 2014.

Anders, A. M., Roe, G. H., Hallet, B., Montgomery, D. R., Finnegan, N. J., and Putkonen, J.: Spatial patterns of precipitation and topography in the Himalaya, Tectonics, Climate, and Landscape Evolution, 398, 39–53, https://doi.org/10.1130/2006.2398(03), 2006.

Armijo, R., Tapponnier, P., Mercier, J. L., and Han, T. L.: Quaternary Extension in Southern Tibet – Field Observations and Tectonic Implications, J. Geophys. Res.-Solid, 91, 13803–13872, https://doi.org/10.1029/JB091iB14p13803, 1986.

Attal, M. and Lavé, J.: Changes of bedload characteristics along the Marsyandi River (central Nepal): Implications for understanding hillslope sediment supply, sediment load evolution along fuvial networks, and denudation in active orogenic belts, Tectonics, Climate, and Landscape Evolution, 143–171, 2006.

Attal, M. and Lavé, J.: Pebble abrasion during fluvial transport: Experimental results and implications for the evolution of the sediment load along rivers, J. Geophys. Res., 114, F04023, https://doi.org/10.1029/2009JF001328, 2009.

Belmont, P., Pazzaglia, F. J., and Gosse, J. C.: Cosmogenic Be-10 as a tracer for hillslope and channel sediment dynamics in the Clearwater River, western Washington State, Earth Planet. Sc. Lett., 264, 123–135, 2007.

Bendick, R. and Ehlers, T. A.: Extreme localized exhumation at syntaxes initiated by subduction geometry, Geophys. Res. Lett., 41, 5861–5867, https://doi.org/10.1002/2014gl061026, 2014.

Bierman, P. and Steig, E.: Estimating rates of denudation using cosmogenic isotope abundances in sediment, Earth Surf. Proc. Land., 21, 125–139, 1996.

Bookhagen, B. and Burbank, D. W.: Topography, relief, and TRMM-derived rainfall variations along the Himalaya, Geophys. Res. Lett., 33, L08405, https://doi.org/10.1029/2006GL026037, 2006.

Bookhagen, B. and Burbank, D. W.: Toward a complete Himalayan hydrological budget: Spatiotemporal distribution of snowmelt and rainfall and their impact on river discharge, J. Geophys. Res., 115, F03019, https://doi.org/10.1029/2009JF001426, 2010.

Bracciali, L., Parrish, R. R., Najman, Y., Smye, A., Carter, A., and Wijbrans, J. R.: Plio-Pleistocene exhumation of the eastern Himalayan syntaxis and its domal "pop-up", Earth-Sci. Rev., 160, 350–385, https://doi.org/10.1016/j.earscirev.2016.07.010, 2016.

Braucher, R., Brown, E., Bourles, D., and Colin, F.: In situ produced Be-10 measurements at great depths: implications for production rates by fast muons, Earth Planet. Sc. Lett., 211, 251–258, https://doi.org/10.1016/S0012-821X(03)00205-X, 2003.

Braucher, R., Merchel, S., Borgomano, J., and Bourles, D. L.: Production of cosmogenic radionuclides at great depth: A multi element approach, Earth Planet. Sc. Lett., 309, 1–9, https://doi.org/10.1016/j.epsl.2011.06.036, 2011.

Brown, E. T., Stallard, R. F., Larsen, M. C., Raisbeck, G. M., and Yiou, F.: Denudation rates determined from the accumulation of in situ-produced [10]Be in the luquillo experimental forest, Puerto Rico, Earth Planet. Sc. Lett., 129, 193–202, https://doi.org/10.1016/0012-821X(94)00249-X, 1995.

Burg, J., Nievergelt, P., Oberli, F., Seward, D., Davy, P., Maurin, J., Diao, Z., and Meier, M.: The Namche Barwa syntaxis: evidence for exhumation related to compressional crustal folding, J. Asian Earth Sci., 16, 239–252, 1998.

Burg, J. P., Davy, P., Nievergelt, P., Oberli, F., Seward, D., Diao, Z. Z., and Meier, M.: Exhumation during crustal folding in the Namche-Barwa syntaxis, Terra Nova, 9, 53–56, https://doi.org/10.1111/j.1365-3121.1997.tb00001.x, 1997.

Carretier, S. and Regard, V.: Is it possible to quantify pebble abrasion and velocity in rivers using terrestrial cosmogenic nuclides?, J. Geophys. Res.-Earth, 116, F04003, https://doi.org/10.1029/2011jf001968, 2011.

Carretier, S., Regard, V., Vassallo, R., Martinod, J., Christophoul, F., Gayer, E., Audin, L., and Lagane, C.: A note on $^{10}$Be-derived mean erosion rates in catchments with heterogeneous lithology: examples from the western Central Andes, Earth Surf. Proc. Land., 40, 1719–1729, https://doi.org/10.1002/esp.3748, 2015a.

Carretier, S., Regard, V., Vassallo, R., Aguilar, G., Martinod, J., Riquelme, R., Christophoul, F., Charrier, R., Gayer, E., Farias, M., Audin, L., and Lagane, C.: Differences in Be-10 concentrations between river sand, gravel and pebbles along the western side of the central Andes, Quat. Geochronol., 27, 33–51, 2015b.

Chirouze, F., Dupont-Nivet, G., Huyghe, P., van der Beek, P., Chakraborti, T., Bernet, M., and Erens, V.: Magnetostratigraphy of the Neogene Siwalik Group in the far eastern Himalaya: Kameng section, Arunachal Pradesh, India, J. Asian Earth Sci., 44, 117–135, https://doi.org/10.1016/j.jseaes.2011.05.016, 2012.

Chmeleff, J., Blanckenburg, F. v., Kossert, K., and Jakob, D.: Determination of the Be-10 half-life by multicollector ICP-MS and liquid scintillation counting, Nucl. Instrum. Meth. B, 268, 192–199, https://doi.org/10.1016/j.nimb.2009.09.012, 2010.

Christl, M., Vockenhuber, C., Kubik, P. W., Wacker, L., Lachner, J., Alfimov, V., and Synal, H. A.: The ETH Zurich AMS facilities: Performance parameters and reference materials, Nucl. Instrum. Meth. B, 294, 29–38, https://doi.org/10.1016/j.nimb.2012.03.004, 2013.

Clapp, E. M., Bierman, P. R., and Caffee, M.: Using Be-10 and Al-26 to determine sediment generation rates and identify sediment source areas in an arid region drainage basin, Geomorphology, 45, 89–104, https://doi.org/10.1016/S0169-555x(01)00191-X, 2002.

Corbett, L. B., Bierman, P. R., and Rood, D. H.: An approach for optimizing in situ cosmogenic Be-10 sample preparation, Quat. Geochronol., 33, 24–34, https://doi.org/10.1016/j.quageo.2016.02.001, 2016.

Delaney, K. B. and Evans, S. G.: The 2000 Yigong landslide (Tibetan Plateau), rockslide-dammed lake and outburst flood: Review, remote sensing analysis, and process modelling, Geomorphology, 246, 377–393, https://doi.org/10.1016/j.geomorph.2015.06.020, 2015.

Delunel, R., van der Beek, P. A., Bourlès, D. L., Carcaillet, J., and Schlunegger, F.: Transient sediment supply in a high-altitude Alpine environment evidenced through a $^{10}$Be budget of the Etages catchment (French Western Alps), Earth Surf. Proc. Land., 39, 890–899, https://doi.org/10.1002/esp.3494, 2014.

Dubille, M. and Lavé, J.: Rapid grain size coarsening at sandstone/conglomerate transition: similar expression in Himalayan modern rivers and Pliocene molasse deposits, Basin Res., 27, 26–42, https://doi.org/10.1111/bre.12071, 2014.

Dunne, J., Elmore, D., and Muzikar, P.: Scaling factors for the rates of production of cosmogenic nuclides for geometric shielding and attenuation at depth on sloped surfaces, Geomorphology, 27, 3–11, 1999.

Enkelmann, E., Ehlers, T. A., Zeitler, P. K., and Hallet, B.: Denudation of the Namche Barwa antiform, eastern Himalaya, Earth Planet. Sc. Lett., 307, 323–333, https://doi.org/10.1016/j.epsl.2011.05.004, 2011.

Finlayson, D., Montgomery, D., and Hallet, B.: Spatial coincidence of rapid inferred erosion with young metamorphic massifs in the Himalayas, Geology, 30, 219–222, https://doi.org/10.1130/0091-7613(2002)030<0219:SCORIE>2.0.CO;230, 2002.

Finnegan, N. J., Hallet, B., Montgomery, D. R., Zeitler, P. K., Stone, J. O., Anders, A. M., and Yuping, L.: Coupling of rock uplift and river incision in the Namche Barwa-Gyala Peri massif, Tibet, Geol. Soc. Am. Bull., 120, 142–155, https://doi.org/10.1130/B26224.1, 2008.

Foster, M. A. and Anderson, R. S.: Assessing the effect of a major storm on (BE)-B-10 concentrations and inferred basin-averaged denudation rates, Quat. Geochronol., 34, 58–68, https://doi.org/10.1016/j.quageo.2016.03.006, 2016.

Frings, R. M.: Downstream fining in large sand-bed rivers, Earth-Sci. Rev., 87, 39–60, https://doi.org/10.1016/j.earscirev.2007.10.001, 2008.

Garzanti, E., Vezzoli, G., Andò, S., France-Lanord, C., Singh, S. K., and Foster, G.: Sand petrology and focused erosion in collision orogens: the Brahmaputra case, Earth Planet. Sc. Lett., 220, 157–174, https://doi.org/10.1016/S0012-821X(04)00035-4, 2004.

Godard, V., Burbank, D. W., Bourles, D. L., Bookhagen, B., Braucher, R., and Fisher, G. B.: Impact of glacial erosion on $^{10}$Be concentrations in fluvial sediments of the Marsyandi catchment, central Nepal, J. Geophys. Res., 117, F03013, https://doi.org/10.1029/2011JF002230, 2012.

Godard, V., Bourles, D. L., Spinabella, F., Burbank, D. W., Bookhagen, B., Fisher, G. B., Moulin, A., and Leanni, L.: Dominance of tectonics over climate in Himalayan denudation, Geology, 42, 243–246, https://doi.org/10.1130/G35342.1, 2014.

Goswami, D. C.: Brahmaputra River, Assam, India – Physiography, Basin Denudation, and Channel Aggradation, Water Resour. Res., 21, 959–978, https://doi.org/10.1029/WR021i007p00959, 1985.

Granger, D., Kirchner, J., and Finkel, R.: Spatially averaged long-term erosion rates measured from in situ-produced cosmogenic nuclides in alluvial sediment, J. Geol., 104, 249–257, 1996.

Heisinger, B., Lal, D., Jull, A., Kubik, P., Ivy-Ochs, S., Knie, K., and Nolte, E.: Production of selected cosmogenic radionuclides by muons: 2. Capture of negative muons, Earth Planet. Sc. Lett., 200, 357–369, 2002a.

Heisinger, B., Lal, D., Jull, A., Kubik, P., Ivy-Ochs, S., Neumaier, S., Knie, K., Lazarev, V., and Nolte, E.: Production of selected cosmogenic radionuclides by muons: 1. Fast muons, Earth Planet. Sc. Lett., 200, 345–355, 2002b.

Hetzel, R., Dunkl, I., Haider, V., Strobl, M., von Eynatten, H., Ding, L., and Frei, D.: Peneplain formation in southern Tibet predates the India-Asia collision and plateau uplift, Geology, 39, 983–986, https://doi.org/10.1130/G32069.1, 2011.

Hydraulics, D.: Delft Hydraulics and Danish Hydraulics Institute, River Survey Project, Flood Action Plan 24, Water Resour. Plann. Org., Dhaka, 1996.

Jain, A. K. and Thakur, V. C.: Abor Volcanics of Arunachal Himalaya, J. Geol. Soc. India, 19, 335–349, 1978.

Jarvis, A., Reuter, A., Nelson, A., and Guevara, E.: Hole-filled SRTM for the globe Version 4, available from the CGIAR-CSI SRTM 90 m Database (http://srtm.csi.cgiar.org), 2008.

Jerolmack, D. J. and Brzinski, T. A.: Equivalence of abrupt grain-size transitions in alluvial rivers and eolian sand seas: A hypothesis, Geology, 38, 886–886, 2010.

King, G. E., Herman, F., and Guralnik, B.: Northward migration of the eastern Himalayan syntaxis revealed by OSL thermochronometry, Science, 353, 800–804, https://doi.org/10.1126/science.aaf2637, 2016.

Klein, M. G., Gottdang, A., Mous, D. J. W., Bourles, D. L., Arnold, M., Hamelin, B., Aumaitre, G., Braucher, R., Merchel, S., and Chauvet, F.: Performance of the HVE 5 MV AMS system at CEREGE using an absorber foil for isobar suppression, Nucl. Instrum. Meth. B, 266, 1828–1832, https://doi.org/10.1016/j.nimb.2007.11.077, 2008.

Kober, F., Hippe, K., Salcher, B., Ivy-Ochs, S., Kubik, P. W., Wacker, L., and Hahlen, N.: Debris-flow-dependent variation of cosmogenically derived catchment-wide denudation rates, Geology, 40, 935–938, https://doi.org/10.1130/G33406.1, 2012.

Kong, P., Na, C. G., Fink, D., Ding, L., and Huang, F. X.: Erosion in northwest Tibet from in-situ-produced cosmogenic Be-10 and Al-26 in bedrock, Earth Surf. Proc. Land., 32, 116–125, https://doi.org/10.1002/esp.1380, 2007.

Koons, P. O., Zeitler, P. K., and Hallet, B.: 5.14 Tectonic Aneurysms and Mountain Building A2, in: Treatise on Geomorphology, edited by: Shroder, J. F., Academic Press, San Diego, 2013.

Korschinek, G., Bergmaier, A., Faestermann, T., Gerstmann, U. C., Knie, K., Rugel, G., Wallner, A., Dillmann, I., Dollinger, G., von Gostomski, C. L., Kossert, K., Maiti, M., Poutivtsev, M., and Remmert, A.: A new value for the half-life of Be-10 by Heavy-Ion Elastic Recoil Detection and liquid scintillation counting, Nucl. Instrum. Meth. B, 268, 187–191, https://doi.org/10.1016/j.nimb.2009.09.020, 2010.

Kuenen, P. H.: Realms of Water, Geogr. J., 122, 266–266, 1956.

Lal, D.: Cosmic ray labeling of erosion surfaces: in situ nuclide production rates and erosion models, Earth Planet. Sc. Lett., 104, 424–439, 1991.

Lal, D., Harris, N. B. W., Sharma, K. K., Gu, Z. Y., Ding, L., Liu, T. S., Dongal, W. Q., Caffee, M. W., and Jull, A. J. T.: Erosion history of the Tibetan Plateau since the last interglacial: constraints from the first studies of cosmogenic Be-10 from Tibetan bedrock, Earth Planet. Sc. Lett., 217, 33–42, https://doi.org/10.1016/S0012-821x(03)00600-9, 2004.

Lang, K. A., Huntington, K. W., and Montgomery, D. R.: Erosion of the Tsangpo Gorge by megafloods, Eastern Himalaya, Geology, 41, 1003–1006, https://doi.org/10.1130/G34693.1, 2013.

Lang, K. A., Huntington, K. W., Burmester, R., and Housen, B.: Rapid exhumation of the eastern Himalayan syntaxis since the late Miocene, Geol. Soc. Am. Bull., 128, 1403–1422, https://doi.org/10.1130/B31419.1, 2016.

Larsen, I. J. and Montgomery, D. R.: Landslide erosion coupled to tectonics and river incision, Nat. Geosci., 5, 468–473, https://doi.org/10.1038/ngeo1479, 2012.

Le Roux-Mallouf, R., Godard, V., Cattin, R., Ferry, M., Gyeltshen, J., Ritz, J. F., Drupka, D., Guillou, V., Arnold, M., Aumaitre, G., Bourles, D. L., and Keddadouche, K.: Evidence for a wide and gently dipping Main Himalayan Thrust in western Bhutan, Geophys. Res. Lett., 42, 3257–3265, https://doi.org/10.1002/2015gl063767, 2015.

Li, Y. K., Li, D. W., Liu, G. N., Harbor, J., Caffee, M., and Stroeven, A. P.: Patterns of landscape evolution on the central and northern Tibetan Plateau investigated using in-situ produced Be-10 concentrations from river Sediments, Earth Planet. Sc. Lett., 398, 77–89, https://doi.org/10.1016/j.epsl.2014.04.045, 2014.

Liu, G. and Einsele, G.: Sedimentary History of the Tethyan Basin in the Tibetan Himalayas, Geol. Rundsch., 83, 32–61, https://doi.org/10.1007/Bf00211893, 1994.

Lukens, C. E., Riebe, C. S., Sklar, L. S., and Shuster, D. L.: Grain size bias in cosmogenic nuclide studies of stream sediment in steep terrain, J. Geophys. Res.-Earth, 121, 978–999, https://doi.org/10.1002/2016jf003859, 2016.

Lupker, M., Blard, P. H., Lave, J., France-Lanord, C., Leanni, L., Puchol, N., Charreau, J., and Bourles, D.: Be-10-derived Himalayan denudation rates and sediment budgets in the Ganga basin, Earth Planet. Sc. Lett., 333, 146–156, https://doi.org/10.1016/j.epsl.2012.04.020, 2012.

Maheo, G., Leloup, P. H., Valli, F., Lacassin, R., Arnaud, N., Paquette, J. L., Fernandez, A., Haibing, L., Farley, K. A., and Tapponnier, P.: Post 4 Ma initiation of normal faulting in southern Tibet. Constraints from the Kung Co half graben, Earth Planet. Sc. Lett., 256, 233–243, https://doi.org/10.1016/j.epsl.2007.01.029, 2007.

Morell, K. D., Sandiford, M., Rajendran, C. P., Rajendran, K., Alimanovic, A., Fink, D., and Sanwal, J.: Geomorphology reveals active decollement geometry in the central Himalayan seismic gap, Lithosphere, 7, 247–256, https://doi.org/10.1130/L407.1, 2015.

Nibourel, L., Herman, F., Cox, S. C., Beyssac, O., and Lave, J.: Provenance analysis using Raman spectroscopy of carbonaceous material: A case study in the Southern Alps of New Zealand, J. Geophys. Res.-Earth, 120, 2056–2079, https://doi.org/10.1002/2015jf003541, 2015.

Niemi, N. A., Oskin, M., Burbank, D. W., Heimsath, A. M., and Gabet, E. J.: Effects of bedrock landslides on cosmogenically determined erosion rates, Earth Planet. Sc. Lett., 237, 480–498, https://doi.org/10.1016/j.epsl.2005.07.009, 2005.

Nishiizumi, K., Imamura, M., Caffee, M. W., Southon, J. R., Finkel, R. C., and McAninch, J.: Absolute calibration of Be-10 AMS standards, Nucl. Instrum. Meth. B, 258, 403–413, https://doi.org/10.1016/j.nimb.2007.01.297, 2007.

Olen, S. M., Bookhagen, B., and Hoffmann, B.: Understanding erosion rates in the Himalayan orogen: A case study from the Arun Valley, J. Geophys. Res.-Earth, 120, 2080–2102, https://doi.org/10.1002/2014jf003410, 2015.

Olen, S. M., Bookhagen, B., and Strecker, M. R.: Role of climate and vegetation density in modulating denudation rates in the Himalaya, Earth Planet. Sc. Lett., 445, 57–67, https://doi.org/10.1016/j.epsl.2016.03.047, 2016.

Phillips, F. M., Argento, D. C., Balco, G., Caffee, M. W., Clem, J., Dunai, T. J., Finkel, R., Goehring, B., Gosse, J. C., Hudson, A. M., Jull, A. J. T., Kelly, M. A., Kurz, M., Lal, D., Lifton, N., Marrero, S. M., Nishiizumi, K., Reedy, R. C., Schaefer, J., Stone, J. O. H., Swanson, T., and Zreda, M. G.: The CRONUS-Earth Project: A synthesis, Quat. Geochronol., 31, 119–154, https://doi.org/10.1016/j.quageo.2015.09.006, 2016.

Portenga, E. W. and Bierman, P. R.: Understanding Earth's eroding surface with [10]Be, GSA Today, 21, 4–10, https://doi.org/10.1130/g111a.1, 2011.

Portenga, E. W., Bierman, P. R., Duncan, C., Corbett, L. B., Kehrwald, N. M., and Rood, D. H.: Erosion rates of the Bhutanese Himalaya determined using in situ-produced [10]Be, Geomorphology, 233, 112–126, https://doi.org/10.1016/j.geomorph.2014.09.027, 2015.

Puchol, N., Lavé, J., Lupker, M., Blard, P.-H., Gallo, F., and France-Lanord, C.: Grain-size dependent concentration of cosmogenic $^{10}$Be and erosion dynamics in a landslide-dominated Himalayan watershed, Geomorphology, 224, 55–68, https://doi.org/10.1016/j.geomorph.2014.06.019, 2014.

Rades, E. F., Hetzel, R., Strobl, M., Xu, Q., and Ding, L.: Defining rates of landscape evolution in a south Tibetan graben with in situ-produced cosmogenic Be-10, Earth Surf. Proc. Land., 40, 1862–1876, https://doi.org/10.1002/esp.3765, 2015.

Raup, B., Racoviteanu, A., Khalsa, S. J. S., Helm, C., Armstrong, R., and Arnaud, Y.: The GLIMS geospatial glacier database: A new tool for studying glacier change, Glob. Planet. Change, 56, 101–110, https://doi.org/10.1016/j.gloplacha.2006.07.018, 2007.

Rosenkranz, R., Spiegel, C., Schildegen, T., and Wittmann, H.: Erosion rates in the rainiest place on earth: cosmogenic $^{10}$Be data from the Shillong Plateau, Himalaya-Karakorum-Tibet workshop, Aussois, 2016.

Salvi, D., Mathew, G., and Kohn, B.: Rapid exhumation of the upper Siang Valley, Arunachal Himalaya since the Pliocene, Geomorphology, 284, 238–249, https://doi.org/10.1016/j.geomorph.2016.09.032, 2017.

Scherler, D., Bookhagen, B., and Strecker, M. R.: Tectonic control on $^{10}$Be-derived erosion rates in the Garhwal Himalaya, India, J. Geophys. Res.-Earth, 119, 83–105, https://doi.org/10.1002/2013jf002955, 2014.

Seward, D. and Burg, J. P.: Growth of the Namche Barwa Syntaxis and associated evolution of the Tsangpo Gorge: Constraints from structural and thermochronological data, Tectonophysics, 451, 282–289, https://doi.org/10.1016/j.tecto.2007.11.057, 2008.

Singh, S. K. and France-Lanord, C.: Tracing the distribution of erosion in the Brahmaputra watershed from isotopic compositions of stream sediments, Earth Planet. Sc. Lett., 202, 645–662, https://doi.org/10.1016/S0012-821X(02)00822-1, 2002.

Sternberg, H.: Untersuchungen über Langen und Querprofil geschiebeführender Flüsse, Z. Bauw., 25, 483–506, 1875.

Stewart, R. J., Hallet, B., Zeitler, P. K., Malloy, M. A., Allen, C. M., and Trippett, D.: Brahmaputra sediment flux dominated by highly localized rapid erosion from the easternmost Himalaya, Geology, 36, 711–714, https://doi.org/10.1130/G24890A.1, 2008.

Stone, J.: Air pressure and cosmogenic isotope production, J. Geophys. Res., 105, 23753–23759, 2000.

Strobl, M., Hetzel, R., Niedermann, S., Ding, L., and Zhang, L.: Landscape evolution of a bedrock peneplain on the southern Tibetan Plateau revealed by in situ-produced cosmogenic $^{10}$Be and $^{21}$Ne, Geomorphology, 153/154, 192–204, https://doi.org/10.1016/j.geomorph.2012.02.024, 2012.

Vance, D., Bickle, M., Ivy-Ochs, S., and Kubik, P. W.: Erosion and exhumation in the Himalaya from cosmogenic isotope inventories of river sediments, Earth Planet. Sc. Lett., 206, 273–288, https://doi.org/10.1016/S0012-821X(02)01102-0, 2003.

von Blanckenburg, F., Belshaw, N. S., and O'Nions, R. K.: Separation of Be-9 and cosmogenic Be-10 from environmental materials and SIMS isotope dilution analysis, Chem. Geol., 129, 93–99, https://doi.org/10.1016/0009-2541(95)00157-3, 1996.

Wang, P., Scherler, D., Liu-Zeng, J., Mey, J., Avouac, J. P., Zhang, Y., and Shi, D.: Tectonic control of Yarlung Tsangpo Gorge revealed by a buried canyon in Southern Tibet, Science, 346, 978–981, https://doi.org/10.1126/science.1259041, 2014.

West, A. J., Hetzel, R., Li, G., Jin, Z. D., Zhang, F., Hilton, R. G., and Densmore, A. L.: Dilution of Be-10 in detrital quartz by earthquake-induced landslides: Implications for determining denudation rates and potential to provide insights into landslide sediment dynamics, Earth Planet. Sc. Lett., 396, 143–153, https://doi.org/10.1016/j.epsl.2014.03.058, 2014.

Wittmann, H. and von Blanckenburg, F.: The geological significance of cosmogenic nuclides in large lowland river basins, Earth-Sci. Rev., 159, 118–141, https://doi.org/10.1016/j.earscirev.2016.06.001, 2016.

Wobus, C., Heimsath, A., Whipple, K., and Hodges, K.: Active out-of-sequence thrust faulting in the central Nepalese Himalaya, Nature, 434, 1008–1011, 2005.

Yanites, B. J., Tucker, G. E., and Anderson, R. S.: Numerical and analytical models of cosmogenic radionuclide dynamics in landslide-dominated drainage basins, J. Geophys. Res.-Earth, 114, F01007, https://doi.org/10.1029/2008jf001088, 2009.

Yin, A.: Cenozoic tectonic evolution of the Himalayan orogen as constrained by along-strike variation of structural geometry, exhumation history, and foreland sedimentation, Earth-Sci. Rev., 76, 1–131, https://doi.org/10.1016/j.earscirev.2005.05.004, 2006.

Zeitler, P. K., Meltzer, A. S., Koons, P. O., Craw, D., Hallet, B., Chamberlain, C. P., Kidd, W. S. F., Park, S. K., Seeber, L., Bishop, M., and Shroder, J.: Erosion, Himalayan Geodynamics, and the Geomorphology of Metamorphism, GSA Today, 11, 4–9, https://doi.org/10.1130/1052-5173(2001)011andlt;0004:ehgatgandgt;2.0.co;2, 2001.

Zeitler, P. K., Meltzer, A. S., Brown, L., Kidd, W. S. F., Lim, C., and Enkelmann, E.: Tectonics and topographic evolution of Namche Barwa and the easternmost Lhasa block, Tibet, in: Toward an Improved Understanding of Uplift Mechanisms and the Elevation History of the Tibetan Plateau, Nie, J., Horton, B. K., and Hoke, G. D., Geological Society of America, 2014.